

1 **Diagnostic calibration of a hydrological model in a mountain**
2 **area by hydrograph partitioning**

3 Z. H. He¹, F. Q. Tian^{1*}, H. V. Gupta², H. C. Hu¹, H. P.Hu¹

4

5

6 1. State Key Laboratory of Hydrosience and Engineering, Department of Hydraulic
7 Engineering, Tsinghua University, Beijing 100084, China

8 2. Department of Hydrology and Water Resources, The University of Arizona, Tucson,
9 Arizona, 85721, USA

10

11 *Corresponding author information:

12 Email: tianfq@tsinghua.edu.cn

13 Tele: +86 010 6277 3396

14 Fax: +86 010 6279 6971

15

16

17

18 Manuscript submitted to Hydrology and Earth System Sciences

19 2015.03.02

20 **Abstract**

21 Hydrological modeling can exploit informative signatures extracted from long time sequences
22 of observed streamflow for parameter calibration and model diagnosis. In this study we
23 explore the diagnostic potential of hydrograph partitioning for model calibration in mountain
24 areas, where meltwater from snow and glaciers are important sources for river runoff (in
25 addition to rainwater). We propose an index-based method to partition the hydrograph
26 according to dominant runoff water sources, and a diagnostic approach to calibrate a
27 mountain hydrological model. First, by accounting for the seasonal variability of precipitation
28 and the altitudinal variability of temperature and snow/glacier coverage, we develop a set of
29 indices to indicate the daily status of runoff generation from each type of water source (i.e.,
30 glacier meltwater, snow meltwater, rainwater, and groundwater). Second, these indices are
31 used to partition a hydrograph into four parts associated with four different combinations of
32 dominant water sources (i.e., groundwater, groundwater + snow meltwater, groundwater +
33 snow meltwater + glacier meltwater, groundwater + snow meltwater + glacier meltwater +
34 rainwater). Third, the hydrological model parameters are grouped by the associated runoff
35 sources, and each group is calibrated to match the corresponding hydrograph partition in a
36 stepwise and iterative manner. Similar to use of the regime curve to diagnose seasonality of
37 streamflow, the hydrograph partitioning curve based on a dominant runoff water source (more
38 briefly called the partitioning curve, not necessarily continuous) can serve as a diagnostic
39 signature that helps relate model performance to model components. The proposed methods
40 are demonstrated via application of a semi-distributed hydrological model (THREW) to the
41 Tailan River basin (1324 km²) in the Tianshan Mountain of China. Results show that the
42 proposed calibration approach performed reasonably well. Cross validation and comparison to
43 an automatic calibration method indicated its robustness.

44 **1 Introduction**

45 **1.1 Background**

46 Parameter calibration has been singled out as one of the major issues in the application
47 of hydrological models (Johnston and Pilgrim, 1976; Gupta and Sorooshian, 1983; Beven and
48 Binley, 1992; Boyle *et al.*, 2000). Commonly, one or more objective functions are selected as
49 criteria to evaluate the similarity between observed and simulated hydrographs (Nash and
50 Sutcliffe, 1970; Brazil, 1989; Gupta *et al.*, 1998; van Griensven and Bauwens, 2003). As
51 model complexity increases, parameter dimensionality also increases significantly, which
52 makes it much more difficult to calibrate model parameters manually. For this reason,
53 automatic calibration procedures have been developed to identify the optimal parameter set
54 (Gupta and Sorooshian, 1985; Gan and Biftu, 1996; Vrugt *et al.*, 2003a,b). However, due to
55 limitations in process understanding and measurement technologies, one can find different
56 parameter sets within a chosen space that may acceptably reproduce the observed aspects of
57 the catchment system (Sorooshian and Gupta, 1983; Beven and Freer, 2001). This
58 phenomenon, which has been called “equifinality”, causes uncertainty in simulation and
59 prediction (Duan *et al.*, 1992; Beven, 1993, 1996), and highlights the need for methods that
60 are powerful enough to ‘diagnostically’ evaluate and correct models, i.e., that are capable of
61 indicating to what degree a realistic representation of the real world has been achieved and
62 pointing towards how the model should be improved (Spear and Hornberger, 1980; Gupta *et al.*,
63 1998, 2008).

64 Traditional regression-based model evaluation strategies (e.g., based on the use of Mean
65 Squared Error or Nash Sutcliffe Efficiency as performance criteria) are demonstrably poor in
66 their ability to identify the roles of various model components or parameters in the model
67 output (Van Straten and Keesman, 1991; Zhang *et al.*, 2008; Gupta *et al.*, 2008; Yilmaz *et al.*,
68 2008; Hingray *et al.*, 2010), which is due in part to the loss of meaningful information when
69 projecting from the high dimension of the data set (like hydrograph) down to the low (often
70 one) dimension of the measure (Yilmaz *et al.*, 2008; Gupta *et al.*, 2009). A diagnostic
71 evaluation method should match the number of unknowns (parameters) with the number of
72 pieces of information by making use of multiple measures of model performance (Gupta *et al.*,
73 1998, 2008, 2009; Yilmaz *et al.*, 2008). One way to exploit hydrological information is to

74 analyze the spatiotemporal characteristics of hydrological variables that can be related to
75 specific hydrological processes in the form of “signature indices” (Richter *et al.*, 1996;
76 Sivapalan *et al.*, 2003; Gupta *et al.* 2008, Yilmaz *et al.*, 2008). Ideally, a “signature” should
77 represent some “invariant” property of the system, be readily identifiable from available data,
78 directly reflect some system function, and be maximally related to some “structure” or
79 “parameter” in the model.

80 Attention to hydrological signatures, therefore, constitutes the natural basis for model
81 diagnosis (Gupta *et al.*, 2008). Placed in this context, the body of literature on the topic is
82 indeed large. Jothityangkoon *et al.* (2001) proposed a downward approach to evaluate the
83 model’s performance against appropriate signatures at progressively refined time scale.
84 Signatures that govern the evaluation of model complexity are the inter-annual variability,
85 mean monthly variation in runoff (called regime curve), and the flow duration curve (FDC).
86 Farmer *et al.* (2003) evaluated the climate, soil and vegetation controls on the variability of
87 water balance through four signatures: gradient of the annual yield frequency graph, average
88 yield over many years for each month, FDC, and magnitude and shape of the hydrograph.
89 Shamir *et al.* (2005a) described a parameter estimation method based on hydrograph
90 descriptors (total flow, range between the extreme values, monthly rising limb density of the
91 hydrograph, monthly maximum flow and negative/positive change) that characterize
92 dominant streamflow patterns at three timescales (monthly, yearly, and record extent).
93 Detenbeck *et al.* (2005) calculated several hydrologic indices including daily flow indices
94 (mean, median, coefficient of variation, and skewness), overall flood indices (flood frequency,
95 magnitude, duration, and flood timing of various levels), low flow variables (mean annual
96 daily minimum), and ranges of flow percentiles to study the relationship of the streamflow
97 regime to watershed characteristics. Shamir *et al.* (2005b) presented two streamflow indices
98 to describe the shape of the hydrograph (rising/declining limb density, i.e., RLD and DLD)
99 for parameter estimation in 19 basins of United States. Yadav *et al.* (2007) used similarity
100 indices and hydrological signatures (runoff ratio and slope of the FDC) to classify catchments.
101 Westerberg *et al.* (2011) selected several evaluation points on the FDC to calibrate models,
102 and compared two selection methods to evaluate their effects on parameter calibration.

103 Generally, the reported signatures have the following two characteristics: (1) they

104 concentrate on the extraction of hydrologically meaningful information contained in
105 hydrographs, and (2) they focus on either an entire study period or a special continuous
106 section of the entire period. They have occasionally considered temporal variability of runoff
107 components and dominance of different runoff sources during different periods (e.g., the
108 seasonal switching of runoff sources discussed in Tian *et al.*, 2012). However, a hydrograph
109 could be dominated by various components or water sources at different response times
110 (Haberlandt *et al.*, 2001; Eder *et al.*, 2005). Within this in mind, a few studies have explored
111 the use of hydrological information in time dimension for stepwise calibration. For example,
112 Schaepli *et al.* (2005) presented a stepwise calibration method for 7 parameters in a high
113 mountainous area: snow and ice melt degree-day factors were conditioned by mass balance,
114 slow reservoir parameters were determined by base flow, reservoir coefficients were
115 calibrated by summer runoff, and the direct runoff coefficient was used to control discharge
116 during precipitation events. Another notable example is Hingray *et al.* (2010), in which the
117 authors estimated the value of snowmelt degree-day factor in a mountain basin by
118 progressively minimizing the differences between observed and simulated values of different
119 magnitude hydrographs. There are also many other follow up studies.

120 In mountain areas, streamflow is composed of both snow/glacier meltwater and
121 rainwater. The energy-based and temperature-index models are two principal approaches to
122 simulate snow and glacier melt (Rango and Martinec, 1979; Howard, 1996; Kane *et al.*, 1997;
123 Singh *et al.*, 2000; Fierz *et al.*, 2003). To describe significant heterogeneity of temperature,
124 precipitation, snow, and glacier, distributed hydrological models are generally used for
125 precipitation-runoff modeling in mountain regions (Daly *et al.*, 2000; Klok *et al.*, 2001 etc.).
126 Also, the utilization of remotely sensing products of precipitation and snow cover data in the
127 mountain runoff modeling has become more popular in recent years (Swamy and Brivio, 1997;
128 Akyurek *et al.*, 2011; Liu *et al.*, 2012 etc.). Most of these studies report sound simulation
129 results. However, the need to develop an appropriate calibration strategy for
130 precipitation-runoff modeling in mountain areas remains a key issue for two reasons: first, the
131 hydrological processes are usually more complex (with snow/glacier melt and possibly soil
132 freezing/thawing) than those in warmer areas, which implies a larger dimension of parameter
133 (R^p) in the corresponding hydrological model; second, measured data set useful for model

134 identification is usually limited due to a sparse gauge network, which produces a small
135 measurement dimension (R^M) far lower than R^P . To address this problem, related studies are
136 putting effort into two directions. One is to reduce the calibrated R^P by estimating some of the
137 parameters based on basin characteristics *a priori*. For example, Gurtz *et al.* (1999) proposed
138 a parameterization method based on elevation, slope and shading derived from basin terrain.
139 Gomez-Landesa and Rango (2002) obtained model parameters of ungauged basins from
140 gauged basins by basin size, proximity of location, and shape similarities. Eder *et al.* (2005)
141 estimated most of the parameters *a priori* from basin physiography before an automatic
142 calibration is applied. The parameterization method may involve some uncertainties but be
143 useful for the determination of insensitive parameters.

144 The second direction is to exploit hydrological information from implicit measure data.
145 For instance, Dunn and Colohan (1999) used baseflow data as additional criteria for model
146 evaluation. Mendoza *et al.* (2003) exploited recession-flow data to estimate hydraulic
147 parameters. Stahl *et al.* (2008) used glacier mass balance information combined with stream
148 hydrographs to constrain melt factors. Huss *et al.* (2008) used annual ice volume change data
149 for optimizing melt and radiation factors, and glacier equilibrium line altitude for
150 precipitation correction factors. Schaepli and Huss (2011) integrated the seasonal information
151 of point glacier mass balance for model calibration by modifying the GSM-SOCONT model.
152 Jost *et al.* (2012) introduced glacier volume loss calculated by high-resolution digital
153 elevation models to calibrate hydrologic model. Knowledge acquired from the
154 aforementioned research indicates that the use of additional information (e.g., baseflow,
155 recession flow, and glacier mass balance) can effectively help reduce parameter uncertainty.

156 However, glacier mass data and baseflow data are usually not available in some
157 mountain basins. In these cases, hydrograph partitioning is another possible way to exploit
158 information from available data. Information about dominant hydrological processes
159 contained in a hydrograph can be extracted by hydrograph partitioning or separation; this has
160 long been a topic of interest in hydrology. Several different kinds of methods have been
161 proposed (Pinder and Jones, 1969; McCuen, 1989; Nathan, 1990; Arnold *et al.*, 1995, 1999;
162 Vivoni *et al.*, 2007), which can generally be classified into graphical methods, analytical
163 methods, empirical methods, geochemical methods and automated program techniques

164 (Nejadhashemi *et al.*, 2009). Most of them primarily focus on the partitioning of baseflow and
165 are not capable of identifying more than two components. With the advent of isotope methods,
166 multi-component hydrograph separation models have been developed. However, these models
167 need be run for an extended period of time (usually a minimum of one hydrologic year) for
168 the assumption that the isotopes of components are conserved to hold (Hooper and
169 Shoemaker, 1986) and call for volumes of field data that are seldom available in poorly
170 gauged and difficult to access mountain basins.

171 **1.2 Objectives and Scope**

172 This paper explores the benefits of partitioning the hydrograph into several parts, each
173 related to one combination of dominant water sources for runoff generation. The parameter
174 group controlling each type of runoff generation is then calibrated using the corresponding
175 partitioning hydrographic curves via a stepwise approach, and model deficiencies are
176 diagnosed by evaluating the model simulations associated with each partitioning curve (as a
177 diagnostic signature). We demonstrate the potential of this approach in a mountain area where
178 streamflow is the result of complex runoff generation processes arising from combinations of
179 storm events and snow/glacier melt. The influence of each type of water source (groundwater,
180 snow meltwater, glacier meltwater, or rainwater) varies in time and can be determined by an
181 analysis of the dynamic spatiotemporal information in the available data series.

182 The paper is organized as follows. Section 2 contains a description of the geographic
183 and hydrological characteristics of the study basin, including the main data sources and data
184 preprocessing. Section 3 details the proposed method of hydrograph partitioning and
185 parameter calibration based on a semi-distributed model coupled with the temperature-index
186 method. Section 4 presents the results and discusses the possible sources of uncertainty.
187 Section 5 provides a summary of this study and discusses further applications of the
188 partitioning strategy.

189 **2 Study Area and Data**

190 **2.1 Overview of the Study Area**

191 The study mountain area (Tailan River basin, TRB) is on the south slope of the Tianshan
192 Mountain (one of the highest mountain areas in China) in the Xinjiang Uygur Autonomous
193 Region of China and extends from 41° 35'N to 42° 05' N and 80° 04'E to 80° 35'E, covering a

194 drainage area of 1324 km². Elevation ranges from 1600 m to 7100 m a.s.l. with an average
195 value as high as 4100 m a.s.l. Precipitation occurs mainly in summer and rarely in winter, and
196 winter precipitation always comes in the form of snowfall. Snow coverage accumulates in
197 winter and ablates from spring into late summer when it melts away completely; the snow
198 coverage dynamics can be obtained from MODIS data (see Fig. 4). The basin is highly
199 glacierized with approximately 33% of the basin area covered by glacier ice (see Fig. 1). The
200 glacier coverage stretches from approximately 3000 m to 7100 m a.s.l. and exists mainly at an
201 altitude range of 4000 m to 5000 m a.s.l. Glacier melt and snowmelt form runoff as long as
202 the temperature rises above a certain threshold and provide primary sources for downstream
203 discharge.

204 TRB is a heavily studied mountain watershed in northwestern China. The relevant
205 literature (Kang and Zhu, 1980; Shen *et al.*, 2003; Xie *et al.*, 2004; Gao *et al.*, 2011; Sun *et al.*,
206 2012) are reviewed below, and the main conclusions about the hydrometeorological
207 characteristics are summarized as follows:

208 (1) The climate presents strong altitudinal variability. The mean annual precipitation in
209 higher mountain areas is approximately 1200 mm (Kang *et al.*, 1980), while it is
210 approximately only 180 mm in the outlet plain area (Xie *et al.*, 2004). The mean annual
211 temperature ranges from below 0°C in mountain areas to approximately 9°C at the basin
212 outlet (Sun *et al.*, 2012).

213 (2) Meltwater is the principal source of streamflow. Snow and glacier meltwater account
214 for approximately 63% of the annual runoff (Kang *et al.*, 1980). The contribution of rainwater
215 is relatively lower and occurs mainly in the storm rain period (May to September) (Xie *et al.*,
216 2004). Groundwater baseflow is smaller but dominates the streamflow in the winter (January,
217 February and December), during which either rainfall or melt rarely occur (Kang *et al.*, 1980).

218 (3) The TRB river network is a simple fan system. Given large topographic drop and
219 moderate drainage area, the runoff concentration time is no longer than one day (Xie *et al.*,
220 2004). Melting and falling water can quickly flow into the main channel and reach the basin
221 outlet.

222 **2.2 Data & Preprocessing**

223 The Tailan gauging station (THS, 1602 m a.s.l.) is located the outlet of the watershed,

224 where runoff, precipitation and temperature have been measured since 1957. To collect
225 temperature and precipitation data at higher elevation, two automatic weather stations (AWS,
226 product type TRM-ZS2) were set up in June 2011 (i.e., XT AWS, at 2116 m a.s.l. and TG
227 AWS, at 2381 m a.s.l.). This relatively short record (from July 1, 2011-December 31, 2012)
228 was used to estimate the lapse rate of precipitation and temperature (see below). The Bingtan
229 automatic weather station (BT AWS, at 3950 m a.s.l.) located in an adjacent catchment
230 (Kumalak basin) was used to validate the estimated temperature lapse rates. A digital
231 elevation model (DEM) with a spatial resolution of 30 m was provided by the International
232 Scientific & Technical Data Mirror Site, Computer Network Information Center of the
233 Chinese Academy of Sciences (<http://www.gscloud.cn>). Remotely sensed snow cover area
234 (SCA) data were downloaded from the MODIS website; the MOD10A2 and MYD10A2
235 products were used, both of which have a spatial resolution of 500m and a temporal
236 resolution of eight-days. Daily snow cover data was obtained by linear interpolation of the
237 eight-day data. The China Glacier Inventory (CGI) (Shi, 2008) was used to derive glacier
238 coverage in the TRB. In our experience, most of the snow melts away after the warm summer
239 period and the lowest snow/ice coverage in the year should, therefore, be roughly equal to the
240 glacier coverage. Based on an analysis of filtered MODIS SCA (see Sect. 2.2.3), the lowest
241 values of snow/ice coverage in the study period (2003-2012) are almost the same, which
242 indicates that TRB glacier coverage is relatively stable during the study period. The DEM,
243 river system, gauging stations and glacier distribution are shown in Fig.1.

244 **2.2.1 Temperature Lapse Rate**

245 Altitudinal distribution of temperature can be estimated through the lapse rate (Rango and
246 Martinec, 1979; Tabony, 1985). According to Aizen *et al.* (2000), rates of temperature
247 decrease with increasing elevation are quite different in various months, and ignoring this
248 difference may lead to significant errors in the simulation of snow accumulation and melt.
249 The lapse rate was therefore estimated for each month. Temperature variations with altitude
250 can be estimated by the following equation, i.e.:

$$251 \quad T = T_o + T_p \cdot (H - h) \quad (1)$$

252 where, T_o is the temperature value at low altitude (THS in this study), and T_p is the

253 temperature lapse rate (usually negative), H and h are the elevation values at high and low
254 positions, i.e., the mean elevation of two AWS and the elevation of THS, respectively. The
255 values of T_p in different months are obtained by minimizing the error function, i.e.:

$$256 \quad \min : z = \sum (T_i - (T_{oi} + T_p \cdot (H - h)))^2 \quad (2)$$

257 where, i indicates the i^{th} day in the analyzed month, T_i is the observed temperature in AWS,
258 which is the mean value of the TG AWS and XT AWS in this study.

259 The temperature series data from July 1, 2011 to December 31, 2012 at THS, TG AWS
260 and XT AWS were used to estimate the temperature lapse rate. The results (Table 1) indicate
261 significant month-to-month variation ranging from $-0.30^\circ\text{C} 100 \text{ m}^{-1}$ in December to -0.86°C
262 100 m^{-1} in August. To validate the temperature lapse rates, the estimated and observed
263 temperature data at BT AWS were compared (Fig. 2). We also compared the estimated
264 temperature by an annual constant lapse rate ($-0.62^\circ\text{C} 100 \text{ m}^{-1}$, a similar value to previous
265 studies, e.g., Tabony (1985) and Tahir *et al.* (2011)). This constant value is optimized by the
266 same method in Eqn. (2) but using all daily temperature measurements. Figure 2 indicates that
267 the monthly lapse rate method performs better than the annual constant rate method at the BT
268 station for all months throughout the year. Further, the temperature curves estimated by
269 monthly lapse rates for April to August match the observed ones rather well. Note that the
270 estimated temperatures tend to underestimate observed ones for the rest of the months, which,
271 however, will not affect the melt runoff significantly due to the general freezing condition
272 during this period.

273 **2.2.2 Precipitation Lapse Rate**

274 Based on the precipitation series measured at THS, the monthly precipitation to annual
275 precipitation ratio (Fig.3) for the study period (2003-2012) indicates that precipitation occurs
276 mainly in May to September. The lapse rate of precipitation was also estimated monthly, and
277 a similar procedure as temperature was applied. The different is that the precipitation analysis
278 was conducted at a weekly rather than daily time step, and the maximum measured
279 precipitation of the two installed AWS was used instead of the mean value. The analyzed
280 period is limited to the storm rain period (May to September). Other months are not included
281 due to the relatively small precipitation amount. The weekly precipitation lapse rates are

282 listed in Table 2. Daily precipitation differences between higher and lower altitudes can be
283 estimated as the weekly precipitation lapse multiplied by the ratio of daily precipitation to the
284 corresponding weekly amount in THS. The precipitation lapse rate was not validated against
285 BT AWS because of significant differences in precipitation distribution between the two
286 basins (i.e., Tailan and Kumalak).

287 **2.2.3 Filtering of MODIS Snow Cover Area Data**

288 Snow cover extent was obtained from MODIS products. The MOD10A2 and MYD10A2
289 products were downloaded from the website <http://reverb.echo.nasa.gov>. In total, we obtained
290 460 eight-day images (two tiles, h23v04 and h24v04) from 2003 to 2012 for each product.
291 Given that the accuracy of the MODIS SCA product is affected by cloud coverage to a
292 significant degree, the remotely sensed images should be filtered to avoid the noise from
293 clouds before using it for hydrological modeling (Ackerman *et al.*, 1998). The following three
294 successive steps are adopted to filter the products based on previous reports (Gafurov and
295 Bardossy, 2009; Wang *et al.*, 2009; Lopez-Burgos *et al.*, 2012):

296 (1) Satellite combination: The snow cover products of two satellites, Terra (MOD10A2)
297 and Aqua (MYD10A2) were combined. As long as the value of a pixel is marked as snow in
298 either satellite, the pixel value is marked as snow.

299 (2) Spatial combination: Inspecting the values of the nearest four pixels around one
300 center pixel marked as cloud, if at least three of the four surrounding pixels are marked as
301 snow, the center pixel is modified as snow.

302 (3) Temporal combination: If one pixel is marked as cloud, its values in the previous and
303 following observations are investigated. If both of the two observed values are snow, then the
304 present value of the same pixel is snow.

305 As an example, the filtered results from year 2004-2005 shown in Fig.4 demonstrate a
306 significant reduction in fluctuation of the SCA products. We find that the lowest values of
307 snow/ice coverage in all years (2003-2012) are relatively stable (from 2003 to 2012 are: 35%,
308 34%, 39%, 36%, 37%, 34%, 41%, 35%, 38%, 39%, showing no obvious trend), which is
309 close to the glacier coverage area (33%) derived from the CGI data mentioned in Sect.2.2. As
310 mentioned before, MODIS snow/ice covered area in later summer is mainly composed of
311 glacier coverage when snow has been melt away completely. The filtered results indicate a

312 relatively stable coverage of glacier in TRB.

313 **2.2.4 Altitudinal Cumulative Melt Curve**

314 The daily temperature of each cell in MODIS SCA images can be estimated by a
315 temperature lapse rate based on its elevation and daily temperature measured at THS. As long
316 as the temperature exceeds a specific threshold value for melt (assumed to be 0°C in this
317 study), a given cell was labeled as an active cell in terms of melt. The land cover type for each
318 cell was classified into glacier, snow, and other land cover according to the CGI and MODIS
319 SCA product. To obtain the area covered by snow only, we subtracted the glacier area in CGI
320 from the SCA (a similar procedure can be found in Luo *et al.*, 2013). When a glacier or snow
321 cover cell is active, it is labeled as a melt cell, and the melt area is computed as the number of
322 active cells multiplied by the area of a cell.

323 Organizing the melt area by elevation from low to high and summing the melt area at
324 each elevation, we can get the altitudinal cumulative melt curve, which can be used to
325 describe the spatiotemporal distribution of melt area. The altitudinal cumulative melt curves
326 calculated from 2003 to 2012 for all months (Fig.5) show that melt mainly occur from May to
327 September, which coincides with the precipitation period. Snowmelt starts at an elevation of
328 approximately 1650 m a.s.l., while glacier melt starts at an elevation of approximately 2950 m
329 a.s.l, which has an important implication for hydrograph partitioning.

330 **3 Methodology**

331 Theoretically, every drop of water in the streamflow comes ultimately from precipitation.
332 Practically, we can consider water sources for runoff generation in mountain areas as mainly
333 consisting of meltwater from snow and glacier, rainwater, and groundwater. Groundwater at
334 the basin scale is recharged by direct infiltration and run-on infiltration of meltwater or
335 rainwater, and it is mainly discharged as baseflow via a subsurface flow path (especially in
336 mountain areas where the large elevation gradient favors baseflow discharge). For the purpose
337 of hydrograph partitioning, we can consider recharge to be a separate water source for
338 streamflow, independent of meltwater and rainwater, which principally forms the baseflow
339 part of a hydrograph. The remaining part of a hydrograph is principally formed by meltwater
340 and rainwater via surface flow path (Blöschl *et al.*, 2013). We develop three indices to
341 indicate the water sources for runoff generation at the daily time scale. The hydrograph is

342 further partitioned into several sub-parts based on the indices values. Each sub-part is
343 dominated by one or more water sources for runoff generation. With the partitioning
344 hydrographic curves, the parameters of hydrological models are correspondingly grouped by
345 runoff sources and calibrated in a stepwise fashion. We use the THREW model coupled with
346 a temperature-index module as an exploratory tool. To better demonstrate usefulness of the
347 proposed methods, only the runoff generation related parameters, which are also significantly
348 sensitive parameters (see Sect.4.6), are calibrated. Other insensitive parameters are fixed at
349 their initial values, specified *a priori* from the literature or by expert knowledge.

350 **3.1 An Index-based Method for Hydrograph Partitioning**

351 In mountain areas, the relative contribution of different runoff water sources to the total
352 streamflow varies throughout the year (Martinec *et al.*, 1982; Dunn and Colohan, 1999; Yang
353 *et al.*, 2007). For the rainwater source, Fig. 3 shows that precipitation in TRB presents strong
354 seasonality and primarily concentrates (more than 76%) in the storm rain period from May to
355 September. During the relatively dry period from October to April, mean precipitation gauged
356 at the THS is just 43 mm, while precipitation in the higher mountainous region is mainly
357 snowfall. Therefore, surface runoff induced by rainwater can rarely occur during relative dry
358 period. It is reasonable to assume that the rainwater source can only contribute to the surface
359 runoff part of a hydrograph on the same day during the storm rain period (May to September)
360 except for the baseflow occurring much later.

361 For the meltwater sources, the altitudinal cumulative melt curves (Fig. 5) show that the
362 areas experiencing glacier melt and snowmelt change significantly with elevation. Melt of
363 glacier and snow begins at different elevations in different months, i.e., glacier melt can only
364 occur in the areas higher than 2950 m (the lower elevation limit of glacier coverage) while
365 snowmelt can occur in areas higher than 1650 m. It can be deduced that snowmelt generally
366 occurs at lower elevations than glacier melt. Remember that temperature decreases with
367 increase in altitude. There should exist a period of time during which temperature at 1650 m
368 is higher than snowmelt threshold while temperature above 2950 m is lower than glacier
369 threshold and thus snow melt does occur but glacier melt not.

370 The groundwater source should be a dominant source for the baseflow part of a
371 hydrograph and, of course, it dominates the recession limb of a hydrograph (part of a

372 baseflow partition) when no rainfall or melting occurs.

373 Based on the above physical understanding, we can partition the hydrograph using the
374 following three indices:

375 (1) Date index (D_i): D_i is used to distinguish the dates on which rainfall and thus
376 possible rainwater directly runoff process occurs. For simplicity, in this study we use
377 D_i to distinguish dry period and storm rain period and assume no rainfall runoff in
378 the dry period, i.e.,

$$379 \quad D_i = \begin{cases} 1, & \text{for days in storm rain period from May to September} \\ 0, & \text{for days in relative dry period from October to April} \end{cases} \quad (3)$$

380 (2) Snowmelt index (S_i): S_i indicates whether snowmelt possibly occurs on a
381 given day:

$$382 \quad S_i = \begin{cases} 1, & \text{for days when temperature at altitude 1650 m is higher than } 0^\circ \text{C} \\ 0, & \text{for other days} \end{cases} \quad (4)$$

383 (3) Glacier melt index (G_i): G_i is used to identify days when glacier melt
384 possibly occurs:

$$385 \quad G_i = \begin{cases} 1, & \text{for days when temperature at altitude 2950 m is higher than } 0^\circ \text{C} \\ 0, & \text{for other days} \end{cases} \quad (5)$$

386 The hydrograph is then partitioned according to the three indices by using the following
387 rules:

$$388 \quad Q = \begin{cases} Q_{SB} & \text{for } S_i=0, G_i=0, \text{ and } D_i = 0 \\ Q_{SB} + Q_{SM} & \text{for } S_i=1, G_i=0, \text{ and } D_i = 0 \\ Q_{SB} + Q_{SM} + Q_{GM} & \text{for } S_i=1, G_i=1, \text{ and } D_i = 0 \\ Q_{SB} + Q_{SM} + Q_{GM} + Q_R & \text{for } D_i = 1 \end{cases} \quad (6)$$

389 where, Q is the overall streamflow series, Q_{SB} stands for the baseflow generated by
390 groundwater source, Q_{SM} for snow meltwater runoff, Q_{GM} for glacier meltwater runoff, and
391 Q_R for rainwater directly runoff. The partitioning principles are described as follows:

392 (1) Groundwater is the dominant component ($Q=Q_{SB}$) when both melt and rainwater
393 directly runoff do not occur. This condition requires $S_i=0$, $G_i=0$, and $D_i=0$;

394 (2) Snow meltwater and groundwater are the dominant components ($Q=Q_{SB}+Q_{SM}$) when
395 the temperature is higher than 0°C at 1650 m a.s.l. and lower than 0°C at 2950 m a.s.l.
396 (requires $S_i=1$, $G_i=0$, and $D_i=0$);

397 (3) Snow meltwater and glacier meltwater coupled with groundwater dominate
398 ($Q=Q_{SB}+Q_{SM}+Q_{GM}$) on days when the temperature at 2950 m a.s.l. exceeds 0°C in October to
399 April. This means $G_i=1$, $D_i=0$, and $S_i=1$, noting that S_i must be equal to 1 when $G_i=1$ for the
400 decreasing nature of temperature along altitude;

401 (4) Finally, all sources are mixed ($Q=Q_{SB}+Q_{SM}+Q_{GM}+Q_R$) for other days in the storm
402 rain period (May to September, $D_i=1$). Each category contains days that could be continuous
403 or discontinuous in time and could lie within different weeks due to temporal variability of
404 precipitation and temperature.

405 3.2 Tsinghua Representative Elementary Watershed Hydrological Model

406 The Tsinghua Representative Elementary Watershed model (THREW model) used for
407 the hydrological simulation in this study, has been successfully applied in many watersheds in
408 both China and the United States (see Tian *et al.*, 2008, 2012; Li *et al.*, 2012; Liu *et al.*, 2012
409 etc.), including an application to a high mountainous catchment of Urumqi River basin by
410 Mou *et al.* (2008). The THREW model adopts the REW (Representative Elementary
411 Watershed) approach to conceptualize a watershed, where REW is the sub-catchment unit for
412 hydrological modeling. The study basin was divided into several units (REW) based on a
413 digital elevation model. Sub-catchment units were further divided into a surface and
414 sub-surface layer, each layer containing several sub-zones. The sub-surface layer is composed
415 of two zones: saturated zone and unsaturated zone, and the surface layer consists of six zones:
416 vegetated zone, bare soil zone, snow covered zone, glacier covered zone, sub-stream-network
417 zone, and main channel reach; see Tian *et al.* (2006) for further details.

418 The main runoff generation processes simulated by the THREW model include rainfall
419 surface runoff, groundwater baseflow, snowmelt and glacier melt. Rainfall surface runoff is
420 simulated by a Xin'anjiang module, which adopts a water storage capacity curve to describe
421 non-uniform distribution of water storage capacity of a sub-catchment (Zhao, 1992). The
422 storage capacity curve is determined by two parameters (spatial averaged storage capacity W_M
423 and shape coefficient B). Rainfall surface runoff forms on areas where storage is replete.
424 Replete areas are calculated by the antecedent storage and current rainfall. The saturation
425 excess runoff is computed based on water balance. The remainder of rainfall can infiltrate into
426 soil and become additional contributions to groundwater. Groundwater forms baseflow that is

427 separately calculated by two coefficients (K_A and K_D). K_A and K_D are outflow coefficients of
428 groundwater storage. Their sum determines the flow rate of groundwater baseflow and their
429 ratio (K_D/K_A) dominate the proportion of free groundwater storage. Infiltration and storage
430 should have effects on the calibration of the two parameters. The Xin'anjiang module has
431 been successfully applied to the Qiedeke, Kaidu, Manasi and Kahai basins in Tianshan
432 Mountain by different authors (Jiang, 1987; Yang *et al.*, 1987; Mu and Jiang, 2009), which
433 indicates its applicability in our study area.

434 For the simulation of melt processes in this study, the THREW model was modified to
435 couple with the temperature-index method, given the easy accessibility of air temperature data
436 and generally good model performance of the temperature-index model (Hock, 2003; Singh *et al.*,
437 2000). Snow and glacier melt are simulated using separate degree-day factors (snowmelt
438 degree day factor D_s and glacier melt degree day factor D_g). Glacier melt only occurs in
439 glacier area according to CGI, which remains stable during the study period (2003-2012, see
440 discussion in Sect. 2.2.3). Precipitation in the snow and glacier zone is divided into rainfall
441 and snowfall according to two threshold temperature values (0°C and 2.5°C are adopted in
442 this study according to Wu and Li (2007)), i.e., when temperature is higher than 2.5°C , all
443 precipitation is rainfall, when temperature is lower than 0°C , all precipitation is snowfall, and
444 when temperature falls between the two thresholds, precipitation is divided into rainfall and
445 snowfall half by half (a simple division scheme adopted here). Rainfall on glacier areas forms
446 runoff and flows into the stream-network directly without infiltration into soil. Snow water
447 equivalent (SWE) on glacier areas is updated by combining snowfall and snowmelt, and for
448 simplicity, snow is assumed to cover all glacier areas when the corresponding SWE is not
449 zero. Snowmelt in glacier areas is simulated using snow degree-day factor D_s until it melts
450 away completely. Snow cover area in non-glacier area is updated using MODIS data. To be
451 noted, snowfall in each subcatchment is calculated according to the daily precipitation and
452 temperature. And snowmelt is simulated using the degree-day method. However, the snow
453 water equivalent in the snow cover zone (non-glacier area) is not computed. The existing of
454 snow cover in each subcatchment is only determined by MODIS snow image. When the
455 MODIS image indicates the existing of snow cover and meanwhile the daily temperature is
456 higher than 0°C , then snowmelt will occur, otherwise, snowmelt will not occur. The

457 identification of snow cover by MODIS image is in accordance with the fact that the
458 partitioning of snowmelt dominant hydrograph is based on MODIS snow products. If the
459 existing of snow cover is determined by snow water equivalent, the temperature parameters to
460 calculate snowfall can have significant effects on the estimation of the degree-day factor for
461 snowmelt. To partly reduce this effect, we calibrate the degree-day factor for snowmelt on the
462 basis of MODIS snow cover products. Although in this way, the water balance of snow cover
463 is not taken into account in the snow cover zone, it should not impact the calibration of the
464 degree-day factor for snowmelt. Since MODIS SCA products (i.e., MYD10A2) are available
465 from 2003, the model simulation period is from 2003 to 2012, of which 2003-2007 for
466 calibration and 2008-2012 for evaluation. The time step for simulation is daily.

467 **3.3 Stepwise Calibration of Grouped Parameters Upon Partitioning Curves**

468 Model parameters are grouped *a priori* according to their connection with causal
469 physical mechanisms (see Table 3). According to Xie *et al.* (2004) and Kang *et al.* (1980),
470 parameters that control groundwater baseflow, snowmelt, glacier melt, and rainwater surface
471 runoff should be the most sensitive parameters for the runoff simulation (also see our
472 sensitivity analysis in Sect. 4.6). These parameters are subjected to calibration in this study.
473 They are related to the corresponding hydrograph parts and then calibrated in a stepwise
474 manner: first, groundwater baseflow parameters (K_A and K_D) are estimated based on the Q_{SB}
475 part of the hydrograph. Second, snowmelt degree day factor (D_s) is calibrated upon the
476 $Q_{SB}+Q_{SM}$ part. Third, glacier melt degree-day factor (D_g) is determined according to the
477 $Q_{SB}+Q_{SM}+Q_{GM}$ part. Finally, rainfall surface runoff parameters (B , W_M) are calibrated on days
478 when D_i equals to 1, i.e., the $Q_{SB}+Q_{SM}+Q_{GM}+Q_R$ part of hydrograph.

479 In each step, only the specific parameter group is subjected to calibration. The
480 parameters determined in the previous steps are kept constant, and all other parameters that
481 will be calibrated in the next steps adopt their initial values. As the simulation in each step can,
482 to some degree, be affected by the initial conditions produced in the preceding step, an
483 iterative procedure is implemented to progressively minimize this influence. The parameter
484 groups are first calibrated based on the corresponding hydrograph parts, and then the stepwise
485 sequence is repeated until the calibrated parameters converge, i.e., the difference in parameter
486 values between two contiguous iterations is less than 10%. In each calibration step, we use

487 $RMSEln$ (Eqn. (7), emphasizing low flow) or $RMSE$ (Eqn. (8), emphasizing high flow) as
 488 objective function for parameter optimization. The remaining, insensitive, parameters are
 489 determined *a priori* according to previous modeling experience (mainly from Sun *et al.*
 490 (2012)) and listed in Table 3. The initial values of the calibrated parameters are also
 491 determined *a priori* according to Sun *et al.* (2012) and Tian *et al.* (2012).

492 The overall streamflow can be simulated with all calibrated parameters, which is
 493 evaluated with NSE and $NSEln$ (logarithm Nash Criterion) values. Given that it is relatively
 494 easier to obtain high evaluation merit values in snowmelt driven basins due to strong
 495 seasonality of streamflow, we further adopt a simple benchmark model (the inter-annual mean
 496 value for every calendar day) to evaluate performance of the proposed method by subtracting
 497 streamflow seasonality. This benchmark model is proposed by Schaepli and Gupta (2007) for
 498 basins having a relatively constant seasonality. The improvement of a model comparing to the
 499 benchmark model is quantified by the BE , see Eqn. (9) for detail.

$$500 \quad RMSEln = \sqrt{\frac{1}{n} \sum_{i=1}^n (\log Q_{obs}(i) - \log Q_{sim}(i))^2} \quad (7)$$

$$501 \quad RMSE = \sqrt{\frac{1}{n} \sum_{i=1}^n (Q_{obs}(i) - Q_{sim}(i))^2} \quad (8)$$

$$502 \quad BE = 1 - \frac{\sum_{i=1}^n (Q_{obs}(i) - Q_{sim}(i))^2}{\sum_{i=1}^n (Q_{obs}(i) - Q_{ben}(i))^2} \quad (9)$$

503 **4 Results and Discussion**

504 **4.1 Partitioning Hydrographic Curves**

505 The hydrograph from 2003 to 2012 was partitioned based on Eqn. (6). In total, we
 506 obtained four kinds of partitioning curves, i.e. Q_{SB} part, $Q_{SB}+Q_{SM}$ part, $Q_{SB}+Q_{SM}+Q_{GM}$ part
 507 and $Q_{SB}+Q_{SM}+Q_{GM}+Q_R$ part. As an example, the partitioning curves in 2003 are shown in Fig.
 508 6, in which the melting period ranges from late February to late November (labeled as red and
 509 green dots). Snowmelt (red dots) starts in February and ends in November, while glacier melt
 510 (green dots) starts later (March) and stops earlier (October). This melt situation agrees well
 511 with the previous studies of Kang *et al.* (1980) and Sun *et al.* (2012). Hydrograph parts
 512 dominated by groundwater source mainly fall into December, January and February and are

513 denoted by black dots. The rainwater surface runoff occurs in the storm rain period only (May
514 to September, denoted by blue dots). The total number of days of $Q_{SB}+Q_{SM}$ part from 2003 to
515 2007 is 365, and that of $Q_{SB}+Q_{SM}+Q_{GM}$ part is 249, while the $Q_{SB}+Q_{SM}+Q_{GM}+Q_R$ part
516 occupies 765 days. The numbers of non-melt days (i.e. the Q_{SB} part, due to glacier melt
517 generally occurs in the $Q_{SB}+Q_{SM}+Q_{GM}+Q_R$ part) in the five years are 114, 80, 89, 96, and 68,
518 respectively. Correspondingly, the mean temperatures in those years gauged at the THS are
519 8.9, 10.1, 9.9, 10.4, and 11.3°C, respectively. A lower mean annual temperature causes a
520 longer non-melt period in that year and vice versa. Note that the partitioning curves can be
521 discontinuous in time due to the spatial-temporal variability of temperature.

522 **4.2 Model Calibration by the Stepwise Method**

523 The six key parameters (K_A , K_D , D_s , D_g , W_M , and B) were firstly calibrated by the
524 proposed stepwise and iterative method. To focus on baseflow generated by the groundwater
525 source during the Q_{SB} period, the $RMSEln$ metric that emphasizes low flow is chosen as the
526 evaluation criterion for the calibration of parameters K_A and K_D . Conversely, high flow is our
527 focus for the remaining periods ($Q_{SB}+Q_{SM}$, $Q_{SB}+Q_{SM}+Q_{GM}$, $Q_{SB}+Q_{SM}+Q_{GM}+Q_R$) and the
528 $RMSE$ metric is chosen as the evaluation criterion for calibration of parameters D_s , D_g , and
529 W_M and B . To deal with interaction between steps, an iterative calibration approach was
530 adopted. A total of five iterations was implemented until the parameter estimates became
531 stable; the simulation of each kind of partitioning curve in each step of the last iteration is
532 presented in Fig. 7. The calibrated parameters are shown in Table 4 and the evaluation merits
533 are listed in Table 5.

534 Figure 7a shows that the magnitude of baseflow in Q_{SB} part was captured well at most of
535 the times. The $RMSEln$ merit is 0.302 m³/s, and the parameters K_A and K_D were determined as
536 1.1 and 0.002 respectively. Streamflow in the $Q_{SB}+Q_{SM}$ part is dominated by both snow
537 meltwater and groundwater. The Fig. 7b shows that melt peak flow events have also been
538 captured well by a calibrated D_s as 2.5 mm °C⁻¹ day⁻¹ after the determination of K_A and K_D in
539 the first step. For the $Q_{SB}+Q_{SM}+Q_{GM}$ part, glacier meltwater began to control the streamflow
540 in combination with snow meltwater and groundwater. Snowmelt and baseflow were
541 determined *a priori* by previously calibrated parameters. The remaining residual between the
542 simulated and observed discharge can be attributed to glacier melt alone, which was thus used

543 for the calibration of glacier melt factor D_g . The $RMSE$ value for this hydrograph partition
544 was optimized as $4.784 \text{ m}^3/\text{s}$ and we obtained a sound simulation by a calibrated D_g as 7.2
545 $\text{mm } ^\circ\text{C}^{-1} \text{ day}^{-1}$ as shown in Fig. 7c. During the storm rain periods ($Q_{SB}+Q_{SM}+Q_{GM} +Q_R$ part),
546 rainwater directly runoff is an additional important component of river runoff. Similarly,
547 parameters W_M and B can be calibrated separately after *priori* determination of melt runoff
548 and groundwater baseflow. The simulated $RMSE$ value in this period is $12.650 \text{ m}^3/\text{s}$, with
549 calibrated $W_M=10.50 \text{ cm}$ and $B=0.80$. The overall daily streamflow simulation is obtained by
550 combining the four partitions together (see Figure 8a). The corresponding NSE index is 0.881
551 and $NSEln$ is 0.929 . Generally the results suggest a sound simulation compared to the
552 observation.

553 To be noted, the calibrated values of melt degree day factors D_s ($2.5 \text{ mm } ^\circ\text{C}^{-1} \text{ day}^{-1}$) and
554 D_g ($7.2 \text{ mm } ^\circ\text{C}^{-1} \text{ day}^{-1}$) are similar to the values obtained in other studies in Tainshan area, e.g.,
555 D_s is calibrated as $2.5 \text{ mm } ^\circ\text{C}^{-1} \text{ day}^{-1}$ by Liu *et al.* (2012), and D_s and D_g are estimated as 3.1
556 $\text{mm } ^\circ\text{C}^{-1} \text{ day}^{-1}$ and $7.3 \text{ mm } ^\circ\text{C}^{-1} \text{ day}^{-1}$ respectively based on observed mass balance data by Liu
557 *et al.* (1999), which indicates the robustness of our calibration method.

558 4.3 Comparison to Automatic Calibration Method

559 For comparison, we also carry out an automatic calibration with the help of the
560 ε -NSGAI algorithm, an optimization method developed by Deb *et al.* (2002) and Kollat and
561 Reed (2006). The six parameters were calibrated together and evaluated by NSE value of the
562 overall hydrograph. The run time of the automatic algorithm is about 5 weeks (840 hour on a
563 desktop equipped with an Intel Core i7 CPU with 2.8GHz). The NSE value for the final
564 optimized parameters is 0.868 , and the $NSEln$ value is 0.846 (Fig. 8b), both of which are
565 lower than the values obtained by the proposed stepwise method. The parameters calibrated
566 by ε -NSGAI are listed in Table 4, and are different from those calibrated by the stepwise
567 method. Specifically, the snowmelt degree-day factor (D_s) and groundwater baseflow
568 parameters (K_A and K_D) obtained by ε -NSGAI are $2.03 \text{ mm } ^\circ\text{C}^{-1} \text{ day}^{-1}$ and 5.6 and 99.1
569 respectively. The evaluation merits of $RMSE$ and $RMSEln$ for each partitioning curve are also
570 shown in Table 5. In general, the simulation by the automatic algorithm is not as good as that
571 by the stepwise method, especially for the low and middle flow partitions ($Q_{SB}+Q_{SM}$ and
572 $Q_{SB}+Q_{SM} +Q_{GM}$). This may be due to the tendency of NSE-based automatic calibration to

573 emphasize high flows.

574 To make a further evaluation, a benchmark model suggested by Schaepli and Gupta
575 (2007) is used for the comparison, which simply simulates daily runoff as the inter-annual
576 daily mean value. Simulation results by the benchmark model are shown in the Figure 8c,
577 which shows *NSE* value as 0.815 and *NSEln* value as 0.923. The high *NSE* and *NSEln* values
578 can be attributed to the strong seasonality of stream discharge in the study basin (Schaepli and
579 Gupta, 2007). The *BE* index (Eqn. (9), see Table 5) is used to measure the improvement of
580 simulations by the calibration methods compared to the benchmark model. A positive value
581 for *BE* means that the evaluated method outperforms the benchmark model. Figure 8 shows
582 the simulations of daily streamflow by the three methods (Fig. 8a by stepwise calibration
583 method, Fig. 8b by automatic calibration method and Fig.8c by benchmark model), which
584 shows better simulation by the two calibration runs with THREW model than the benchmark
585 model (*BE* values are both positive). The stepwise calibration run obtained a *BE* value of
586 0.355, while *BE* of the automatic calibration run is 0.271. The benchmark model describes the
587 mean value of daily discharge on each calendar day. The higher the *BE* value is, the better the
588 seasonal variability of the hydrograph is captured by the evaluation method. The higher *BE*
589 value in the stepwise calibration method can be attributed to the better simulation of middle
590 and low flows which are dominated by groundwater and melt water (Fig.8a). However, *BE*
591 values simulated by two calibrated parameter sets are both relatively low, which is attributed
592 to the poor mimic of the (rapidly rising and falling) peaks.

593 Note that the automatic calibration method based on *NSE* value of the overall
594 hydrograph adopts 1D measurement information to optimize four parameter groups.
595 Benefitting from the partitioning curves, however, the stepwise calibration method increases
596 the dimension of hydrological signature to four. The signature dimension is now equal to the
597 number of parameter groups, and the grouped parameters can be optimized according to their
598 corresponding runoff components separately. A sound simulation of the overall hydrograph is
599 obtained by the reasonable reproduction of the separate partitioning curves. Therefore,
600 parameters calibrated by the stepwise method are inclined to have more explicit physical
601 basis.

602 In regards to computation efficiency, the stepwise calibration required 385 runs of the

603 model to complete, with each model run taking about 1.5 minutes and the total computation
604 time being about 10 hrs. In contrast, the state-of-the-art automatic calibration algorithm
605 required about 5 weeks of CPU time consumption on a desktop equipped with an Intel Core
606 i7 CPU and 2.8GHz. The comparison indicates that the stepwise calibration method is both
607 more physically based as well as more computationally efficient.

608 It is worth noting, the performance of the automatic calibration algorithm can increase if
609 the algorithm keeps on running, and even be higher than that of the step-wise calibration
610 method. The comparison here is intending to show that the step-wise calibration method
611 based on hydrograph partition can achieve considerable performance more effectively. The
612 automatic algorithm here treats all the parameters equally during the calibration period. Each
613 parameter should be optimized when searching for the optimal parameter set. This searching
614 algorithm hampers the efficiency of the calibration procedure without identifying the
615 dominant sub-periods for different parameters. In the step-wise calibration method, only
616 parameters that are responsible for the simulation of corresponding hydrograph partition are
617 optimized in each step. And also the calibration of parameter by this method reflects the role
618 of each parameter for the basin runoff generation.

619 **4.4 Evaluation for the Stepwise Calibration Method**

620 The parameter set calibrated by the stepwise method is applied to the evaluation period
621 (2008~2012), and the daily discharge simulation is shown in Fig. 9a. The evaluation merits
622 are listed in Table 5. The *NSE*, *NSEln* and *RMSE* values for the whole period indicate sound
623 evaluation results but general lower performance compared to calibration period. However,
624 the evaluation results by the stepwise method are still significant better than the benchmark
625 model, which obtained a *NSE* value as low as 0.577 (Fig. 9b and Table 5). The *BE* value in
626 evaluation period by the stepwise calibration method is 0.413. Furthermore, from the partition
627 perspective, the *RMSEln* and *RMSE* values for four partitions in Table 5 show that the low
628 flow simulations (Q_{SB} , $Q_{SB}+Q_{SM}$, and $Q_{SB}+Q_{SM}+Q_{GM}$ parts) are pretty good and even
629 outperform the calibration simulations. The high flow simulation ($Q_{SB}+Q_{SM}+Q_{GM}+Q_R$ part) is,
630 however, insufficient, with *RMSE* 16.727 m³/s (compared to 12.65 m³/s in calibration period).
631 The lower performance of overall evaluation should be attributed to the insufficiency in storm
632 rain days, especially for some extreme storm events in the summer of 2010 (see Fig. 9a). The

633 underestimation of these events is likely due to inadequate observations of rainfall, which are
634 principally due to the strong spatial variability of rainfall in mountainous areas. It is widely
635 acknowledged that the extreme runoff events are difficult to capture in mountain area, where
636 gauged station is scarce, on the daily scale (Aizen *et al.*, 2000; Jasper *et al.*, 2002). However,
637 the accuracy of our results is similar to Li and Williams (2008) (used SRM model) and Liu *et*
638 *al.* (2012) (who used the MIKE-SHE model) who performed similar work in a basin that is
639 close to TRB in Tianshan Mountains. Their Nash values for daily discharge varied from 0.51
640 to 0.78, and also failed to simulate the peak flows in summer. They also attributed the low
641 efficiency to the heavy precipitation.

642 To further evaluate the robustness of the stepwise calibration method based on
643 partitioning curves, cross validation was implemented. The hydrograph in the evaluation
644 period was partitioned based on dominant runoff sources, as was done in the calibration years
645 2003-2007. We calibrated the model to 2008-2012 and evaluated it for 2003-2007. The new
646 calibrated parameter values are $K_A=0.9$, $K_D=0.003$, $D_s=2.2 \text{ mm } ^\circ\text{C}^{-1} \text{ day}^{-1}$, $D_g=7.4 \text{ mm } ^\circ\text{C}^{-1}$
647 day^{-1} , $W_M=10.2 \text{ cm}$ and $B=0.77$, which are similar to the values calibrated in 2003-2007 listed
648 in Table 4. The *NSE*, *NSEln* and *RMSE* values for calibration period 2008-2012 and
649 evaluation period 2003-2007 are 0.757, 0.900, 10.892 m³/s and 0.883, 0.910, 8.589 m³/s,
650 respectively, using this new calibrated parameter set. The simulations of the two periods by
651 cross validation are presented in Fig.9c-d, which shows similar performance by two calibrated
652 parameter sets and further demonstrates the robustness of the proposed stepwise calibration
653 method.

654 **4.5 Sensitivity Analysis on Index-based Partitioning Method**

655 The stepwise calibration method relies heavily on the hydrograph partition for different
656 runoff components. The indices defined in Sect. 3.1 are keys to identify the dominant days for
657 melt water and rainwater. The definitions for elevation bands for the 0 °C Isotherm and for
658 storm rain days in the year producing rainwater runoff should have significant influence on
659 the parameter calibration. In this study, the elevation band of 0 °C Isotherm for snowmelt is
660 fixed and defined as 1650m. This value should have minimal effect on the snowmelt
661 simulation, as the occurrence of snowmelt is actually determined by the MODIS snow cover
662 data. Glacier cover area is assumed as constant, which is very rough for we have only one

663 CGI data. In this section, we define different elevation bands of 0 °C Isotherm for glacier to
664 analyze the effect of glacier area variation on the model calibration. We also select different
665 seasons as the storm rain period to analyze its sensitive effect.

666 According to the CGI data, the glacier area extends from the altitude of 2950m in 2002.
667 Considering the possible variability, we define four different lowest elevation bands for the
668 glacier area (LEG), i.e., -500m (2450m), -200m (2750m), +200m (3150m) and +500m
669 (3450m). As an example, various hydrograph partition patterns in year 2003 are shown in Fig.
670 10. For the storm rain period (SRP), new seasons are defined as April to October, April to
671 September, May to October, and June to August compared to the benchmark period May to
672 September. A new hydrograph partition pattern in year 2003 is also shown in Fig. 10. The left
673 column in Fig. 10 shows that the $Q_{SB}+Q_{SM}+Q_{GM}$ partition becomes longer while the $Q_{SB}+Q_{SM}$
674 partition becomes shorter when the LEG is lower. Therefore, glacier melt starts earlier and
675 ends later in the years with lower LEG. In the right column, the $Q_{SB}+Q_{SM}+Q_{GM}$ partition
676 becomes longer with the shorter SRP, while the variation of the $Q_{SB}+Q_{SM}$ partition can be
677 negligible. Parameters were re-calibrated according to the new partition curves, and the
678 results are shown in Table 6, indicating the increase of degree-day factor for glacier melt (D_g)
679 with the increase of the LEG. The value of D_g is also found to become higher when the SRP
680 falls in the warmer months. The variation of LEG imposes significant impacts on the
681 calibration of D_g , with a result ranging from 5.8 to 8.0 mm °C⁻¹ day⁻¹, while the variation of
682 SRP principally impacts the calibration of parameter W_M , with a result ranging from 8.2 to
683 10.5 cm. However, the *NSE* values (see Table 6) for different settings show minimal
684 differences. This can be attributed to the fact that parameters are optimized on separate
685 partitioning curves in the stepwise calibration method. Each hydrograph partition can be well
686 simulated by adjusting the parameter values. The partition patterns can influence the value of
687 parameters significantly but only slightly influence the discharge simulation. Among various
688 LEGs, the setting of 2950m leads to the highest *NSE* value. Glacier melt degree day factor (D_g)
689 calibrated with this LEG is 7.2 mm °C⁻¹ day⁻¹, which is very close to the value estimated as
690 7.3 mm °C⁻¹ day⁻¹ by Liu *et al.* (1999), in which the D_g is estimated according to the observed
691 glacier mass balance data in Tianshan area. This can further demonstrate the reasonability of
692 the assumption in Sect. 3.2 that the glacier area is stable and its lowest elevation is fixed at

693 2950m during the study period. For the various storm rain periods (SRP), when the May to
694 October period is adopted, the discharge simulation is slightly better than the benchmark
695 setting of SRP, i.e. May to September. This phenomenon seems to indicate the importance of
696 precipitation measurement as discussed in Sect. 4.4. Given that the hydrograph partition in
697 Fig. 6 is on the basis of setting the SRP as May to September, some small rain events in April
698 are not taken into account. Sensitive analysis in Table 6 indicates that taking these events into
699 account (i.e., defining SRP as April to October and April to September), the calibrated value
700 of parameter W_M can be significantly different. With the help of more advanced precipitation
701 measurement, the storm rain period can be determined more precisely to improve the model
702 simulation.

703 To evaluate the relative dominance of multiple runoff components on the total runoff, we
704 compute their contributions to total runoff by various LEG and SRP in Fig.11. The mean
705 contributions of every runoff component are as follows: groundwater contributes 17%, snow
706 meltwater contributes 16.5%, glacier meltwater contributes 40% and rainwater directly runoff
707 contributes 26.5%. Total melt water (snowmelt and glacier melt) occupies approximately 56.5%
708 and is close to the ratio 63% suggested by Kang *et al.* (1980).

709 **4.6 Sensitivity Analysis on Parameters**

710 The number of parameters to be calibrated is determined by the parameter sensitivity and
711 *a priori* analysis. To evaluate the effect of different parameters on the simulation of different
712 hydrograph partitions, we implemented a simple parameter sensitivity procedure that is
713 carried out by a “one-at-a-time” approach. Parameters from different groups in Table 3 are
714 selected for sensitivity analysis, including saturated hydraulic conductivity for u-zone K_s^u ,
715 saturated hydraulic conductivity for s-zone K_s^s , subsurface flow coefficient K_A and K_D ,
716 manning roughness coefficient for hillslope n^t , spatial heterogeneous coefficient for
717 infiltration capacity α^{IFL} , ground surface depression storage capacity $Fmax^b$, shape coefficient
718 to calculate the saturation excess runoff area from the Xin’anjiang model B , spatial averaged
719 tension water storage capacity in the Xin’anjiang model W_M , glacier degree day factor D_g
720 and snowmelt degree per day factor D_s . Parameter are varied from -50% to +50% of the
721 calibrated values using the stepwise method in Table 4. The relative change (R_{MS}) of
722 simulated measure merits ($RMSEln$ or $RMSE$) for different hydrograph partitions are used to

723 evaluate the sensitivity (Eqn. (10)), where MS is the value of measure merits by the calibrated
 724 parameter, MS_+ is the merits value obtained by the parameter +50% of the calibrated one, and
 725 MS_- is the merits value obtained by the parameter -50% of the calibrated one. The sensitivity
 726 simulation results are shown in Table 7, which demonstrates the dominant control of
 727 parameter K_A , K_D , W_M , B , D_s and D_g . Some parameters have significant effects on simulation
 728 of multi hydrograph partitions. For example, parameters controlling the $Q_{SB}+Q_{SM}+Q_{GM}+Q_R$
 729 period can also have significant effect on the other periods. To minimize this interaction,
 730 iterative calibration was implemented in the calibration procedure. The number of calibrated
 731 parameters is determined as six, which control the main runoff components (i.e. groundwater
 732 baseflow, snowmelt, glacier melt and rainwater directly runoff). Note that the low dimension
 733 of parameter calibration should not account for the low efficiency of peak flow simulation,
 734 referring to the similar study in Tianshan mountain areas by Li and Williams (2008), and Liu
 735 *et al.*(2012), in which the models have a higher parameter dimension (higher than six), and
 736 the peak flow simulations are still inadequate.

$$737 \quad R_{MS} = \left| \frac{MS_+ - MS_-}{MS} \right| \times 100\% \quad (10)$$

738 **5 Summary and Conclusion**

739 This study proposes a diagnostic calibration approach to extract hydrological signatures
 740 from available data series in a mountain area, which can be further used to partition the
 741 hydrograph into dominant runoff sources. The parameters of a hydrological model were
 742 grouped according to runoff sources and then related to the corresponding hydrologic
 743 partitioning curve. Each parameter group was calibrated to improve the simulation of the
 744 corresponding partitioning curve in a stepwise way. In this way, the dimension of
 745 hydrological signature is expanded to equal the number of parameter groups. The parameter
 746 uncertainty due to interaction of parameters is reduced via an iterative calibration procedure.
 747 Application to a mountain watershed in the Tianshan Mountain in northwestern China
 748 showed that the approach performed reasonably well. Cross validation and comparison to an
 749 automatic calibration method indicated its applicability.

750 Note that a semi-distributed hydrological model was utilized to illustrate the proposed
 751 diagnostic calibration approach in the high mountainous Tailan River Basin. Glacier mass
 752 balance is not simulated in the model and the glacier coverage was kept fixed during the study

753 period, which can be subject to significant change in the context of global warming.
754 According to existing studies (Stahl *et al.*, 2008; Schaefli and Huss, 2011; Jost *et al.*, 2012),
755 glacier mass balance data is useful to constrain the parameter uncertainty for hydrological
756 modeling in a glaciated basin. While arguing that our assumption of unchanged glacier
757 coverage will not weaken the importance of the proposed approach, we acknowledge that an
758 improved model coupled with glacier mass balance equations will improve the accuracy of
759 hydrological simulation aided by glacier mass balance observations. This is left for future
760 research.

761 A prerequisite for the proposed approach is hydrograph partitioning based on dominant
762 runoff sources. The key to the partition procedure is to identify the functional domain of each
763 runoff source from signature information extracted from easily available data. A partition can
764 be achieved in which the relative roles of different runoff components in the basin runoff vary
765 significantly with time. The mountain watershed is an area in which the runoff source can be
766 separated by the combination of topography, ground-gauged temperature and precipitation,
767 and remotely sensed snow and glacier coverage. Other areas with strong temporal variability
768 of catchment wetness along with precipitation (e.g., monsoon zones) could also be suitable
769 for the proposed approach. The Dunne runoff is prone to dominate the hydrograph when the
770 catchment is wet and it could switch to Hortonian runoff rapidly under the combination of
771 high evaporative demand and less precipitation, as shown by Tian *et al.* (2012) in the Blue
772 River basin of Oklahoma. This is, however, also left for future research.

773 *Acknowledgments.* We wish to thank Mr. Wang Xinhui for his assistance in collecting
774 hydrometeorology data in the Tailan River basin, and thank Charlie Luce and Viviana
775 Lopez-Burgos who provided great help in MODIS snow coverage product filtering. The
776 authors would also like to thank sincerely two Referees (B. Schaepli and M. Zappa) and Editor
777 Markus Weiler for his careful comments, which improve the quality of manuscript significantly.
778 This study was supported by the National Science Foundation of China (NSFC 51190092,
779 U1202232, 51222901) and the foundation of the State Key Laboratory of Hydroscience and
780 Engineering of Tsinghua University (2012-KY-03, 2014-KY-01). Their support is greatly
781 appreciated.

782 **References**

- 783 Ackerman, S. A., Strabala, K. I., Menzel, W. P., Frey, R. A., Moeller, C. C. and Gumley, L.
784 E.: Discriminating clear sky from clouds with MODIS, *J. Geophys. Res.*, 103, 32141-32157,
785 1998.
- 786 Aizen, V., Aizen, E., Glazirin, G. and Loaiciga, H. A.: Simulation of daily runoff in Central
787 Asian alpine watersheds, *J. Hydrol.*, 238, 15-34, 2000.
- 788 Akyurek, Z., Surer, S. and Beser, O.: Investigation of the snow-cover dynamics in the Upper
789 Euphrates Basin of Turkey using remotely sensed snow-cover products and
790 hydrometeorological data, *Hydrol. Process.*, 25 (23), 3637-3648, 2011.
- 791 Arnold, J. G. and Allen, P. M.: Automated methods for estimating baseflow and ground water
792 recharge from streamflow records, *Journal of the American Water Resources Association*,
793 35, 411-424, 1999.
- 794 Arnold, J. G., Allen, P. M., Muttiah, R. and Bernhardt, G.: Automated base-flow separation
795 and recession analysis techniques, *Ground Water*, 33, 1010-1018, 1995.
- 796 Beven, K.: Prophecy, reality and uncertainty in distributed hydrological modelling, *Adv.*
797 *Water Resour.*, 16, 41-51, 1993.
- 798 Beven, K.: Equifinality and uncertainty in geomorphological modelling, *The Scientific Nature*
799 *of Geomorphology: Proceedings of the 27th Binghamton Symposium in Geomorphology*,
800 289-313, 1996.
- 801 Beven, K. and Binley, A.: The future of distributed models-model calibration and uncertainty
802 prediction, *Hydrol. Process.*, 6, 279-298, 1992.
- 803 Beven, K. and Freer, J.: Equifinality, data assimilation, and uncertainty estimation in
804 mechanistic modelling of complex environmental systems using the GLUE methodology, *J.*
805 *Hydrol.*, 249, 11-29, 2001.
- 806 Blöschl, G., Sivapalan, M., Wagener, T., Viglione, A. and Savenije, H. (Eds.): *Runoff*
807 *Prediction in Ungauged Basins: Synthesis Across Processes, Places and Scales*, Cambridge
808 Univ. Press, New York, 2013.
- 809 Boyle, D. P., Gupta, H. V. and Sorooshian, S.: Toward improved calibration of hydrologic
810 models: Combining the strengths of manual and automatic methods, *Water Resour. Res.*,
811 36, 3663-3674, 2000.
- 812 Brazil, L.: Multilevel calibration strategy for complex hydrologic simulation models, NOAA
813 Technical Report, NWS 42, Fort Collins, 217 pp, 1989.
- 814 Bulygina, N., McIntyre, N. and Wheeler, H.: Conditioning rainfall-runoff model parameters
815 for ungauged catchments and land management impacts analysis, *Hydrol. Earth Syst. Sci.*,
816 13 (6), 893-904, 2009.
- 817 Daly, S. F., Davis, R., Ochs, E. and Pangburn, T.: An approach to spatially distributed snow
818 modelling of the Sacramento and San Joaquin basins, California, *Hydrol. Process*, 14
819 (18S1), 3257-3271, 2000.
- 820 Deb, K., Pratap, A., Agarwal, S. and Meyarivan, T.: A fast and elitist multiobjective genetic
821 algorithm: NSGA-II, *IEEE Transactions on evolutionary computation*, 6, 182-197, 2002.
- 822 Detenbeck, N. E., Brady, V. J., Taylor, D. L., Snarski, V. M. and Batterman, S. L.:
823 Relationship of stream flow regime in the western Lake Superior basin to watershed type
824 characteristics, *J. Hydrol.*, 309, 258-276, 2005.
- 825 Duan, Q., Sorooshian, S. and Gupta, V.: Effective and efficient global optimization for

826 conceptual rainfall-runoff models, *Water Resour. Res.*, 28, 1015-1031, 1992.

827 Dunn, S. M. and Colohan, R. J. E.: Developing the snow component of a distributed
828 hydrological model: a step-wise approach based on multi-objective analysis, *J. Hydrol.*,
829 223, 1-16, 1999.

830 Eder, G., Fuchs, M., Nachtnebel, H. and Loibl, W.: Semi-distributed modelling of the
831 monthly water balance in an alpine catchment, *Hydrol. Process.*, 19, 2339-2360, 2005.

832 Farmer, D., Sivapalan, M. and Jothityangkoon, C.: Climate, soil, and vegetation controls upon
833 the variability of water balance in temperate and semiarid landscapes: Downward approach
834 to water balance analysis, *Water Resour. Res.*, 39, 1035, 2003.

835 Fierz, C., Ribet, P., Adams, E., Curran, A., Fohn, P., Lehning, M. and Pluss, C.: Evaluation of
836 snow-surface energy balance models in alpine terrain, *J. Hydrol.*, 282 (1-4), 76-94, 2003.

837 Gafurov, A. and Bardossy, A.: Cloud removal methodology from MODIS snow cover
838 product, *Hydrol. Earth Syst. Sci.*, 13, 1361-1373, 2009.

839 Gan, T. Y. and Biftu, G. F.: Automatic calibration of conceptual rainfall-runoff models:
840 Optimization algorithms, catchment conditions, and model structure, *Water Resour. Res.*,
841 32, 3513-3524, 1996.

842 Gao, W., Li, Z. and Zhang, M.: Study on Particle-size Properties of Suspended Load in
843 Glacier Runoff from the Tomor Peak, *Arid Zone Research*, 28, 449-454, 2011(in Chinese).

844 Gomez-Landesa, E. and Rango, A.: Operational snowmelt runoff forecasting in the Spanish
845 Pyrenees using the snowmelt runoff model, *Hydrol. Process.*, 16, 1583-1591, 2002.

846 Gupta, H. V., Kling, H., Yilmaz, K. K. and Martinez, G. F.: Decomposition of the mean
847 squared error and NSE performance criteria: Implications for improving hydrological
848 modelling, *J. Hydrol.*, 377, 80-91, 2009.

849 Gupta, H. V., Sorooshian, S. and Yapo, P. O.: Toward improved calibration of hydrologic
850 models: Multiple and noncommensurable measures of information, *Water Resour. Res.*, 34,
851 751-763, 1998.

852 Gupta, V. K. and Sorooshian, S.: Uniqueness and observability of conceptual rainfall-runoff
853 model parameters: The percolation process examined, *Water Resour. Res.*, 19, 269-276,
854 1983.

855 Gupta, V. K. and Sorooshian, S.: The Automatic Calibration of Conceptual Catchment
856 Models Using Derivative-Based Optimization Algorithms, *Water Resour. Res.*, 21,
857 437-485, 1985.

858 Gupta, H. V., Wagener, T. and Liu, Y.: Reconciling theory with observations: elements of a
859 diagnostic approach to model evaluation, *Hydrol. Process.*, 22, 3802-3813, 2008.

860 Gurtz, J., Baltensweiler, A. and Lang, H.: Spatially distributed hydrotope-based modelling of
861 evapotranspiration and runoff in mountainous basins, *Hydrol. Process.*, 13, 2751-2768,
862 1999.

863 Haberlandt, U., Klocking, B., Krysanova, V. and Becker, A.: Regionalisation of the base flow
864 index from dynamically simulated flow components - a case study in the Elbe River Basin,
865 *J. Hydrol.*, 248, 35-53, 2001.

866 Hingray, B., Schaefli, B., Mezghani, A. and Hamdi, Y.: Signature-based model calibration for
867 hydrological prediction in mesoscale Alpine catchments, *Hydrolog. Sci. J.*, 55 (6),
868 1002-1016, 2010.

869 Hock, R.: Temperature index melt modelling in mountain areas, *J. Hydrol.*, 282, 104-115,

870 2003.

871 Hooper, R. P. and Shoemaker, C. A.: A Comparison of Chemical and Isotopic Hydrograph
872 Separation, *Water Resour. Res.*, 22, 1444-1454, 1986.

873 Howard, C.: Revisiting the degree-day method for snowmelt computations – Discussion,
874 *Water Resources Bulletin*, 32 (2), 411-413, 1996.

875 Huss, M., Farinotti, D., Bauder, A. and Funk, M.: Modelling runoff from highly glacierized
876 alpine drainage basins in a changing climate, *Hydrol. Process.*, 22 (19SI), 3888-3902, 2008.

877 Jasper, K., Gurtz, J. and Herbert, L.: Advanced flood forecasting in Alpine watersheds by
878 coupling meteorological observations and forecasts with a distributed hydrological model, *J.*
879 *Hydrol.*, 267 (1-2), 40-52, 2002.

880 Jiang, H. F.: Snow ablation modeling and its application to Qiedeke basin, *Journal of*
881 *Xinjiang Agricultural University*, 1, 67-75, 1987 (in Chinese).

882 Johnston, P. R. and Pilgrim, D. H.: Parameter optimization for watershed models, *Water*
883 *Resour. Res.*, 12, 477-486, 1976.

884 Jost, G., Moore, R. D., Menounos, B. and Wheate, R.: Quantifying the contribution of glacier
885 runoff to streamflow in the upper Columbia River Basin, Canada, *Hydrol. Earth Syst. Sci.*,
886 16, 849-860, 2012.

887 Jothityangkoon, C., Sivapalan, M. and Farmer, D. L.: Process controls of water balance
888 variability in a large semi-arid catchment: downward approach to hydrological model
889 development, *J. Hydrol.*, 254, 174-198, 2001.

890 Juston, J., Seibert, J. and Johansson, P.: Temporal sampling strategies and uncertainty in
891 calibrating a conceptual hydrological model for a small boreal catchment, *Hydrol. Process.*,
892 23 (21), 3093-3109, 2009.

893 Kane, D. L., Gieck, R. E., and Hinzman, L. D.: Snow Modeling at Small Alaskan Arctic
894 Watershed, *Journal of Hydrologic Engineering*, 2 (4), 204-210, 1997.

895 Kang, E., Zhu, S. and Huang, M.: Some Results of the Research on Glacial Hydrology in the
896 Region of MT. Tuomuer, *Journal of Glaciology and Geocryology*, 2, 18-21, 1980(in
897 Chinese).

898 Klok, E. J., Jasper, K., Roelofsma, K. P., Gurtz, J. and Badoux, A.: Distributed hydrological
899 modelling of a heavily glaciated Alpine river basin, *Hydrolog. Sci. J.*, 46 (4), 553-570,
900 2001.

901 Kollat, J. B. and Reed, P. M.: Comparing state-of-the-art evolutionary multi-objective
902 algorithms for long-term groundwater monitoring design, *Adv. Water Resour.*, 29, 792-807,
903 2006.

904 Li, H. Y., Sivapalan, M. and Tian, F. Q.: Comparative diagnostic analysis of runoff
905 generation processes in Oklahoma DMIP2 basins: The Blue River and the Illinois River, *J.*
906 *Hydrol.*, 418, 90-109, 2012.

907 Li, X. G. and Williams M. W.: Snowmelt runoff modelling in an arid mountain watershed,
908 Tarim Basin, China, *Hydrol. Process.*, 22 (19SI), 3931-3940, 2008.

909 Liu, D. F., Tian, F. Q., Hu, H. C. and Hu, H. P.: The role of run-on for overland flow and the
910 characteristics of runoff generation in the Loess Plateau, China, *Hydrolog. Sci. J.*, 57,
911 1107-1117, 2012.

912 Liu, S. Y., Xie, Z. C., Wang, N. L. and Ye, B. S.: Mass balance sensitivity to climate change:
913 a case study of glacier no. 1 at Urumqi riverhead, Tianshan mountains, China, *Chin. Geogr.*

914 Sci., 9, 134-140, 1999.

915 Liu, T., Willems, P., Feng, X. W., Li, Q., Huang, Y., Bao, A. M., Chen, X., Veroustraete, F.
916 and Dong, Q. H.: On the usefulness of remote sensing input data for spatially distributed
917 hydrological modelling: case of the Tarim River basin in China, *Hydrol. Process.*, 26 (3),
918 335-344, 2012.

919 Lopez-Burgos, V., Gupta, H. V. and Clark, M.: A probability of snow approach to removing
920 cloud cover from MODIS Snow Cover Area products, *Hydrol. Earth Syst. Sci. Discuss*, 9,
921 13693-13728, 2012.

922 Luo, Y., Arnold, J., Liu, S., Wang, X. and Chen, X.: Inclusion of glacier processes for
923 distributed hydrological modeling at basin scale with application to a watershed in
924 Tianshan Mountains, northwest China, *J. Hydrol.*, 477, 72-85, 2013.

925 Martinec, J., Oeschger, H., Schotterer, U. and Siegenthaler, U.: Snowmelt and groundwater
926 storage in alpine basin, In *Hydrological Aspects of Alpine and High Mountain Areas*,
927 Wallingford, United Kingdom: IAHS Press, 169–175, 1982.

928 McCuen, R. H.: *Hydrologic analysis and design*, Prentice Hall, New Jersey pp.355-360, 1989.

929 Mendoza, G. F., Steenhuis, T. S., Walter, M. T. and Parlange, J. Y.: Estimating basin-wide
930 hydraulic parameters of a semi-arid mountainous watershed by recession-flow analysis, *J.*
931 *Hydrol.*, 279, 57-69, 2003.

932 Mou, L., Tian, F., Hu, H. and Sivapalan, M.: Extension of the Representative Elementary
933 Watershed approach for cold regions: constitutive relationships and an application, *Hydrol.*
934 *Earth Syst. Sci.*, 12, 565-585, 2008.

935 Mu, Z. X. and Jiang, H. F.: Establishment of snowmelt type Xin'anjiang watershed model
936 based on digital elevation model, *Journal of Xinjiang Agricultural University*, 5 (32), 75-80,
937 2009 (in Chinese).

938 Nash, J. E. and Sutcliffe, J. V.: River flow forecasting through conceptual models part I — A
939 discussion of principles, *J. Hydrol.*, 10, 282-290, 1970.

940 Nathan, R. J., McMahon, T. A.: Evaluation of automated techniques for base flow and
941 recession analyses, *Water Resour. Res.*, 26, 1465-1473, 1990.

942 Nejadhashemi, A. P., Shirmohammadi, A., Sheridan, J. M., Montas, H. J. and Mankin, K. R.:
943 Case Study: Evaluation of Streamflow Partitioning Methods, *J. Irrig. Drain. Eng.*, 135,
944 791-801, 2009.

945 Pellicciotti, F., Brock, B., Strasser, U., Burlando, P., Funk, M. and Corripio, J.: An enhanced
946 temperature-index glacier melt model including the shortwave radiation balance:
947 development and testing for Haut Glacier d'Arolla, Switzerland, *Journal of Glaciology*, 51
948 (175), 573-587, 2005.

949 Pinder, G. F. and Jones, J. F.: Determination of the ground-water component of peak
950 Determination of the ground-water component of peak discharge from the chemistry of
951 total runoff, *Water Resour. Res.*, 5, 438-445, 1969.

952 Rango, A. and Martinec, J.: Application of a Snowmelt-runoff Model Using Landsat Data,
953 *Nord. Hydrol.*, 10, 225-238, 1979.

954 Richter, B. D., Baumgartner, J. V., Powell, J. and Braun, D. P.: A method for assessing
955 hydrologic alteration within ecosystems, *Conservation Biology*, 10, 1163-1174, 1996.

956 Schaeffli, B. and Gupta, H. V.: Do Nash values have value, *Hydro. Process.*, 21 (15),
957 2075-2080, 2007.

958 Schaeffli, B., Hingray, B., Niggli, M. and Musy, A.: A conceptual glacio-hydrological model
959 for high mountainous catchments, *Hydrol. Earth Syst. Sci.*, 9 (1-2), 95-109, 2005.

960 Schaeffli, B. and Huss, M.: Integrating point glacier mass balance observations into hydrologic
961 model identification, *Hydrol. Earth Syst. Sci.*, 15, 1227-1241, 2011.

962 Shamir, E., Imam, B., Gupta, H. V. and Sorooshian, S.: Application of temporal streamflow
963 descriptors in hydrologic model parameter estimation, *Water Resour. Res.*, 41, W06021,
964 doi:10.1029/2004WR003409, 2005a.

965 Shamir, E., Imam, B., Morin, E., Gupta, H. V. and Sorooshian, S.: The role of hydrograph
966 indices in parameter estimation of rainfall-runoff models, *Hydrol. Process.*, 19, 2187-2207,
967 2005b.

968 Shen, Y., Liu, S., Ding, Y. and Wang, S.: Glacier Mass Balance Change in Tailanhe River
969 Watersheds on the South Slope of the Tianshan Mountains and its impact on water
970 resources, *Journal of Glaciology and Geocryology*, 25, 124-129, 2003(in Chinese).

971 Shi, Y.: Concise Glacier Inventory of China, Shanghai Popular Science Press., Shanghai,
972 China, 2008(in Chinese).

973 Singh, P., Kumar, N. and Arora, M.: Degree-day factors for snow and ice for Dokriani
974 Glacier, Garhwal Himalayas, *J. Hydrol*, 235, 1-11, 2000.

975 Sivapalan, M., Bloschl, G., Zhang, L. and Vertessy, R.: Downward approach to hydrological
976 prediction, *Hydrol. Process.*, 17, 2101-2111, 2003.

977 Sorooshian, S. and Gupta, V. K.: Automatic calibration of conceptual rainfall-runoff
978 models-the question of parameter observability and uniqueness, *Water Resour. Res.*, 19,
979 260-268, 1983.

980 Spear, R. C. and Hornberger, G. M.: Eutrophication in peel inlet—II. Identification of critical
981 uncertainties via generalized sensitivity analysis, *Water Research*, 14, 43-49, 1980.

982 Stahl, K., Moore, R. D., Shea, J. M., Hutchinson, D. and Cannon, A. J.: Coupled modelling of
983 glacier and streamflow response to future climate scenarios, *Water Resour. Res.*, 44, 2008.

984 Sun, M., Yao, X., Li, Z. and Li, J.: Estimation of Tailan River Discharge in the Tianshan
985 Mountains in the 21st Century, *Advances on Climate Change Research*, 8, 342-349,
986 2012(in Chinese).

987 Swamy, A. N. and Brivio, P. A.: Modelling runoff using optical satellite remote sensing data
988 in a high mountainous alpine catchment of Italy, *Hydrol. Process.*, 11 (11), 1475-1491,
989 1997.

990 Tabony, R. C.: The variation of surface temperature with altitude, *Meteorological Magazine*,
991 114, 37-48, 1985.

992 Tahir, A. A., Chevallier, P., Arnaud, Y., Neppel, L. and Ahmad, B.: Modeling
993 snowmelt-runoff under climate scenarios in the Hunza River basin, Karakoram Range,
994 Northern Pakistan, *J. Hydrol*, 409, 104-117, 2011.

995 Tian, F. Q., Hu, H. P. and Lei, Z. D.: Thermodynamic watershed hydrological model:
996 Constitutive relationship, *Science in China, Ser. E-Technological Sciences*, 51, 1353-1369,
997 2008.

998 Tian, F., Hu, H., Lei, Z. and Sivapalan, M.: Extension of the Representative Elementary
999 Watershed approach for cold regions, *Hydrol. Earth Syst. Sci.*, 10, 619-644, 2006.

1000 Tian, F. Q., Li, H. Y. and Sivapalan, M.: Model diagnostic analysis of seasonal switching of
1001 runoff generation mechanisms in the Blue River basin, Oklahoma, *J. Hydrol*, 418, 136-149,

1002 2012.

1003 Van Griensven, A. and Bauwens, W.: Multiobjective autocalibration for semidistributed
1004 water quality models, *Water Resour. Res.*, 39, 1348, 2003.

1005 Van Straten, G. T. and Keesman, K. J.: Uncertainty propagation and speculation in projective
1006 forecasts of environmental change: A lake-eutrophication example, *J. Forecast.*, 10,
1007 163-190, 1991.

1008 Vivoni, E. R., Entekhabi, D., Bras, R. L. and Ivanov, V. Y.: Controls on runoff generation and
1009 scale-dependence in a distributed hydrologic model, *Hydrol. Earth Syst. Sci.*, 11,
1010 1683-1701, 2007.

1011 Vrugt, J. A., Gupta, H. V., Bastidas, L. A., Bouten, W. and Sorooshian, S.: Effective and
1012 efficient algorithm for multiobjective optimization of hydrologic models, *Water Resour.*
1013 *Res.*, 39, 1214, 2003a.

1014 Vrugt, J. A., Gupta, H. V., Bouten, W. and Sorooshian, S.: A Shuffled Complex Evolution
1015 Metropolis Algorithm for Optimization and Uncertainty Assessment of Hydrological
1016 Model Parameters, *Water Resour. Res.*, 39, 1201, doi:10.1029/2002WR001642, 8., 2003b.

1017 Wang, X. W., Xie, H. J., Liang, T. G. and Huang, X. D.: Comparison and validation of
1018 MODIS standard and new combination of Terra and Aqua snow cover products in northern
1019 Xinjiang, China, *Hydrol. Process.*, 23, 419-429, 2009.

1020 Westerberg, I. K., Guerrero, J. L., Younger, P. M., Beven, K. J., Seibert, J., Halldin, S., Freer,
1021 J. E. and Xu, C. Y.: Calibration of hydrological models using flow-duration curves, *Hydrol.*
1022 *Earth Syst. Sci.*, 15 (7), 2205-2227, 2011.

1023 Wu, J., L. L.: A rain-on-snow mixed flood forecast model and its application, *Engineering*
1024 *Journal of Wuhan University*, 40, 20-23, 2007(in Chinese).

1025 Xie, C., Ding, Y., Liu, S. and Han, H.: Analysis on the Glacial Hydrological Features of the
1026 Glaciers on the South Slope of Mt. Tuomuer and the Effects on Runoff, *Arid Land*
1027 *Geography*, 27, 570-575, 2004(in Chinese).

1028 Yadav, M., Wagener, T. and Gupta, H.: Regionalization of constraints on expected watershed
1029 response behavior for improved predictions in ungauged basins, *Adv. Water Resour*, 30,
1030 1756-1774, 2007.

1031 Yang, D. Q., Zhao, Y. Y., Armstrong, R., Robinson, D. and Brodzik, M. J.: Streamflow
1032 response to seasonal snow cover mass changes over large Siberian watersheds, *J. Geophys.*
1033 *Res.*, 112, F02S22F2, 2007.

1034 Yang, X. S., Jiang, H. F., Huang, C. R. Zheng, Z., and Yong, G.: An applied study on the
1035 snowmelt type of Xin'anjiang watershed model at the Kaidu river basin, *Journal of*
1036 *Xinjiang Agricultural University*, 4, 82-90, 1987 (in Chinese).

1037 Yilmaz, K. K., Gupta, H. V. and Wagener, T.: A process-based diagnostic approach to model
1038 evaluation: Application to the NWS distributed hydrologic model, *Water Resour. Res.*, 44,
1039 W09417, doi:10.1029/2007WR006716, 2008.

1040 Zhang, Z. X., Wagener, T., Reed, P. and Bhushan, R.: Reducing uncertainty in predictions in
1041 ungauged basins by combining hydrologic indices regionalization and multiobjective
1042 optimization, *Water Resour. Res.*, 44 (W00B04), doi:10.1029/2008WR006833, 2008.

1043 Zhao, R. J.: The Xin'anjiang model applied in China, *J. Hydrol*, 135, 371-381, 1992.

1044

Table1. Estimated monthly temperature lapse rate in the TRB

Month	Temperature lapse rate (°C/day/100 m)
January	-0.38
February	-0.38
March	-0.66
April	-0.76
May	-0.80
June	-0.78
July	-0.82
August	-0.86
September	-0.66
October	-0.60
November	-0.54
December	-0.30
Annual	-0.62

1045

1046

Table 2. Estimated week-precipitation lapse rate in storm rain months

Month	Precipitation lapse rate (mm/week/ 100 m)
May	1.63
June	1.69
July	3.14
August	2.40
September	2.28

1047

1048
1049

Table 3. Grouped parameters in the THREW model. Parameters subjected to calibration are highlighted in red.

Category	Symbol	Unit	Description	Value
Subsurface	K_s^u	m s ⁻¹	Saturated hydraulic conductivity for u-zone	1.25E-05
	K_s^s	m s ⁻¹	Saturated hydraulic conductivity for s-zone	1.25E-05
	K_A	-	Coefficient used to calculate subsurface flow	Calibrated
	K_D	-	Coefficient used to calculate subsurface flow	Calibrated
Routing	n^t	-	Manning roughness coefficient for hillslope, obtained from the literature according to land use and vegetation type	1.50E-01
	n^r	-	Similar to n^t , roughness coefficient for channel	3.00E-01
Infiltration	α^{EFL}	-	Spatial heterogeneous coefficient for exfiltration capacity	1.00E+00
	α^{IFL}	-	Spatial heterogeneous coefficient for infiltration capacity	1.50E+00
Interception	$F \max^b$	m	Ground surface depression storage capacity	0.00E+00
	α^{vb}	m	Maximum rainfall depth a single leaf can intercept and hold	1.00E-05
Rainfall runoff	B	-	Shape coefficient to calculate the saturation excess runoff area from the Xin'anjiang model	Calibrated
	W_M	cm	Spatial averaged tension water storage capacity in the Xin'anjiang model	Calibrated
Melt	D_g	mm °C ⁻¹ day ⁻¹	Glacier melt degree day factor	Calibrated
	D_s	mm °C ⁻¹ day ⁻¹	Snowmelt degree day factor	Calibrated

1050

1051

Table 4. Calibrated parameters by the stepwise and automatic methods

Parameter	Stepwise Calibrated	Automatic Calibrated
K_A	1.1	5.6
K_D	0.002	99.1
D_s (mm °C ⁻¹ day ⁻¹)	2.5	2.03
D_g (mm °C ⁻¹ day ⁻¹)	7.2	7.52
W_M (cm)	10.5	11.9
B	0.80	0.62

1052

Table 5. Evaluation merits for the stepwise and automatic calibration methods

Merits	Calibration period	Calibration period	Calibration period	Evaluation period	Evaluation period
	Automatic method	Stepwise method	Benchmark model	Stepwise method	Benchmark model
$RMSEln(Q_{SB}, m^3/s)$	0.352	0.302	-	0.213	-
$RMSE(Q_{SB}+Q_{SM}, m^3/s)$	2.807	1.811	-	1.762	-
$RMSE(Q_{SB}+Q_{SM}+Q_{GM}, m^3/s)$	6.079	4.784	-	4.558	-
$RMSE(Q_{SB}+Q_{SM}+Q_{GM}+Q_R, m^3/s)$	13.245	12.650	-	16.727	-
NSE	0.867	0.881	0.815	0.752	0.577
$NSEln$	0.841	0.929	0.923	0.894	0.844
$RMSE (m^3/s)$	8.990	8.459	10.534	11.021	14.381
BE	0.271	0.355	-	0.413	-

1055 Table 6. Sensitive analysis of the calibrated parameters on lowest elevation band for glacier
 1056 area (LEG) and storm rain period (SRP). *NSE* is the Nash Sutcliffe Efficiency value for the
 1057 calibration period.

	LEG (a.s.l. m)	$D_s(\text{mm/d/}^\circ\text{C})$	$D_g(\text{mm/d/}^\circ\text{C})$	$W_M(\text{cm})$	B	K_A	K_D	NSE
	3450	2.2	8.0	10.1	0.70	0.7	0.002	0.870
	3150	2.5	7.9	10.1	0.75	0.7	0.002	0.871
SRP:	2950	2.5	7.2	10.5	0.80	1.1	0.002	0.881
May. To Sep.	2750	3.0	6.8	10.2	0.75	1.0	0.002	0.880
	2450	2.8	5.8	10.0	0.78	0.8	0.002	0.876
	SRP	$D_s(\text{mm/d/}^\circ\text{C})$	$D_g(\text{mm/d/}^\circ\text{C})$	$W_M(\text{cm})$	B	K_A	K_D	NSE
	Jun. to Aug.	2.9	7.5	8.2	0.75	0.9	0.002	0.871
	May. to Oct.	2.8	6.9	9.4	0.76	0.8	0.002	0.882
LEG=2950m	May. to Sep.	2.5	7.2	10.5	0.80	1.1	0.002	0.881
	Apr. to Sep.	2.2	7.1	8.3	0.75	0.9	0.002	0.878
	Apr. to Oct.	2.6	6.9	9.4	0.77	1.1	0.002	0.881

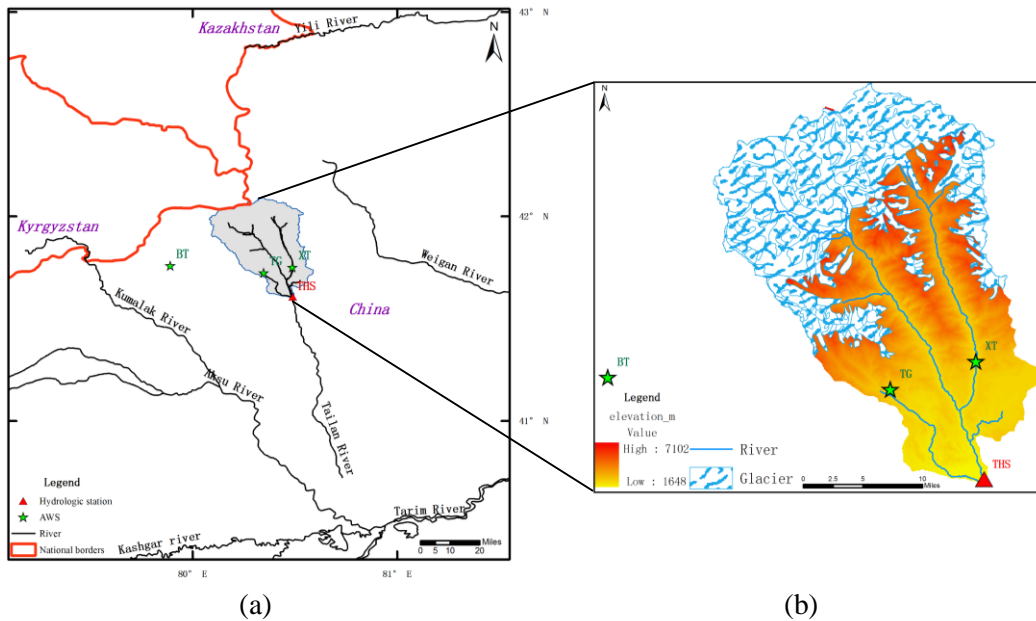
1058

1059
1060

Table 7. R_{MS} (%) for parameter sensitivity (R_{MS} values indicating the most sensitive parameters are labeled in bold and red)

Merits	Subsurface				Routing	Infiltration	Interception	Rainfall Runoff		Melt	
	K_s^u	K_s^s	K_A	K_D	n^t	α^{IFL}	$F \max^b$	W_M	B	D_s	D_g
$RMSE_{ln}$ (Q_{SB})	9.70	11.14	38.44	44.39	15.70	0.12	0.08	1.07	18.51	7.53	2.88
$RMSE$ ($Q_{SB}+Q_{SM}$)	0.32	0.40	11.91	0.06	9.35	0.47	0.14	8.27	25.14	51.22	0.69
$RMSE$ ($Q_{SB}+Q_{SM}+Q_{GM}$)	0.22	0.21	0.62	0.64	10.00	0.17	0.25	7.92	0.29	26.28	40.79
$RMSE$ ($Q_{SB}+Q_{SM}+Q_{GM}+Q_R$)	0.17	0.85	0.57	0.97	1.84	0.08	0.06	19.35	22.48	10.78	11.57

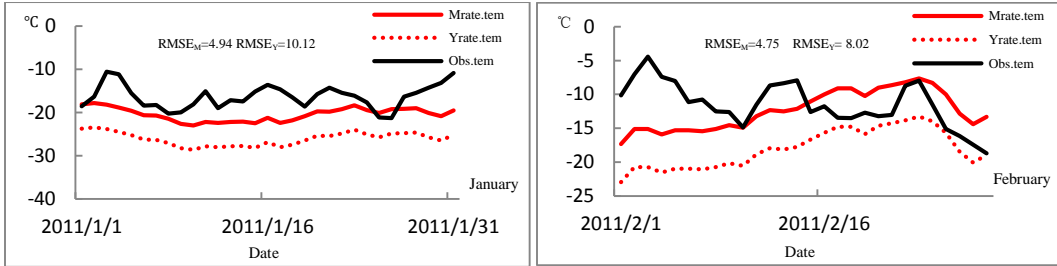
1061



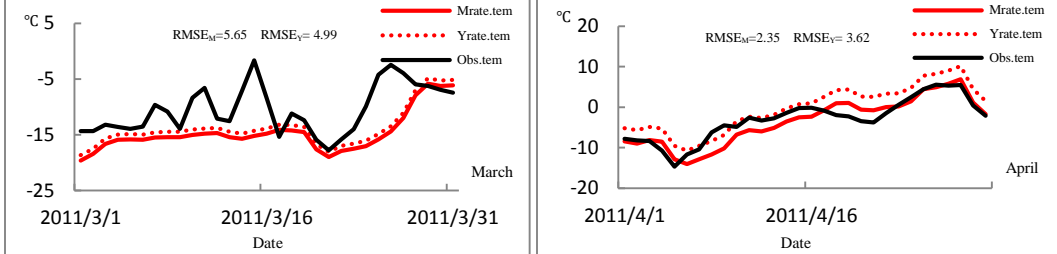
1062
 1063
 1064
 1065
 1066
 1067
 1068
 1069
 1070

Figure 1. Location of the Tailan River basin in Xinjiang Uygur Autonomous Region, China. Two automatic weather stations (TG at 2381 m a.s.l. and XT at 2116 m a.s.l.) were set up in upstream mountain area in July, 2011. Additionally, the BT weather station (3950 m a.s.l.) located in the adjacent Kumalak River basin was used to validate the estimated temperature lapse rates. The Tailan Hydrologic Station (THS) has gauged streamflow data at the catchment outlet since 1957(a). Glacier occupies approximately 33% of the total basin area (b).

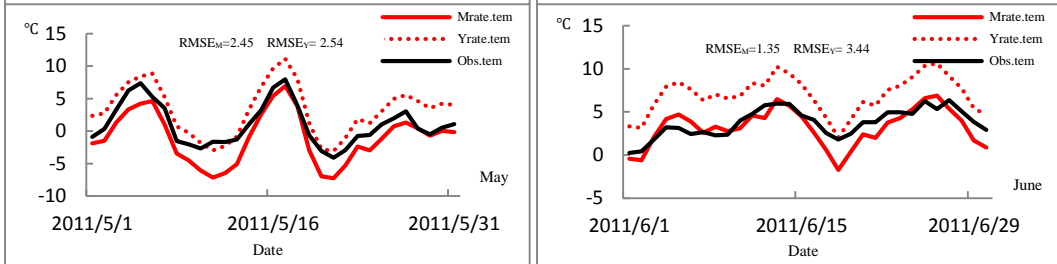
1071



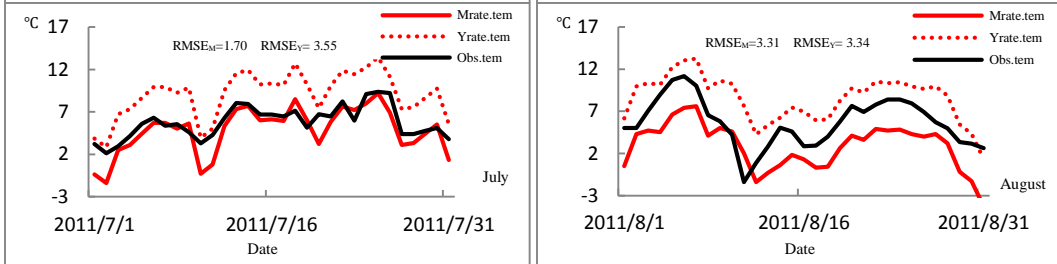
1072



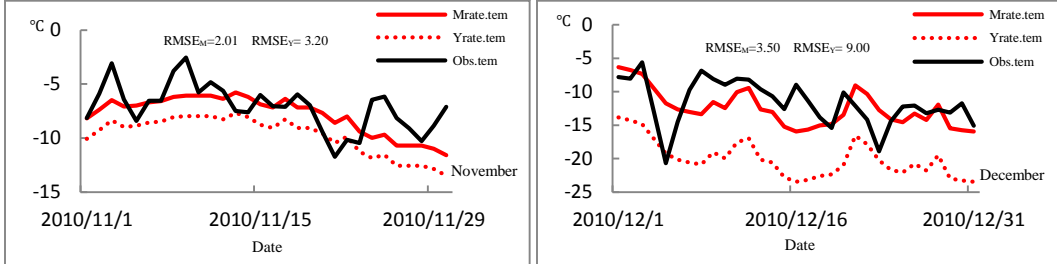
1073



1074



1075



1076

1077

1078

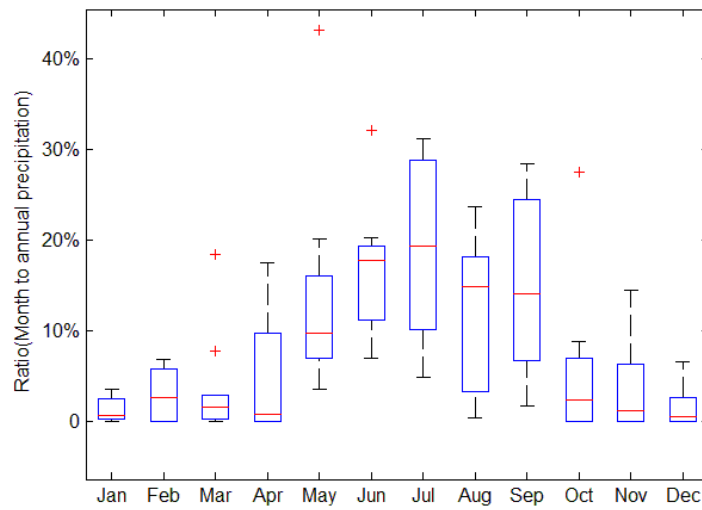
1079

1080

1081

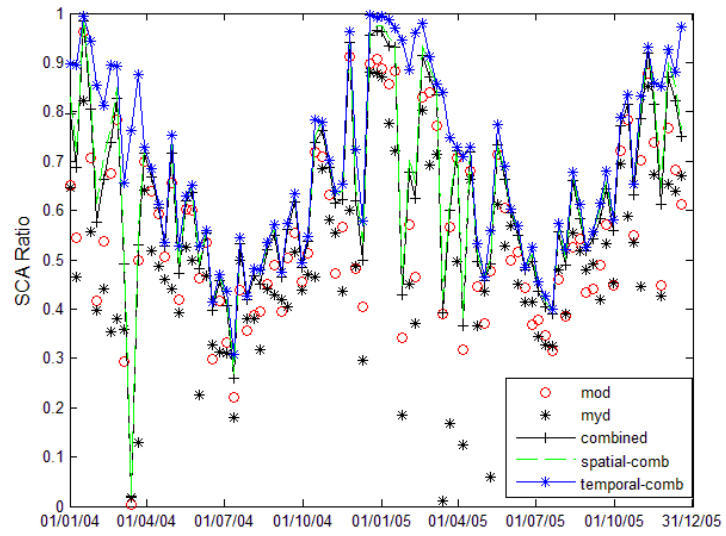
1082

Figure 2. Evaluation of the estimated temperature lapse rate at the BT station. The black solid line is the observed temperature series at BT (Obs.tem); the red solid line is the estimated temperature by monthly lapse rate (Mrate.tem). The red dotted line indicates the estimated temperature based on annual constant rate (Yrate.tem). The goodness of fit between the observed and estimated temperature is measured by $RMSE_M$ for monthly lapse rate and $RMSE_Y$ for annual constant rate, respectively. The temperature series in September and October are absent at BT.



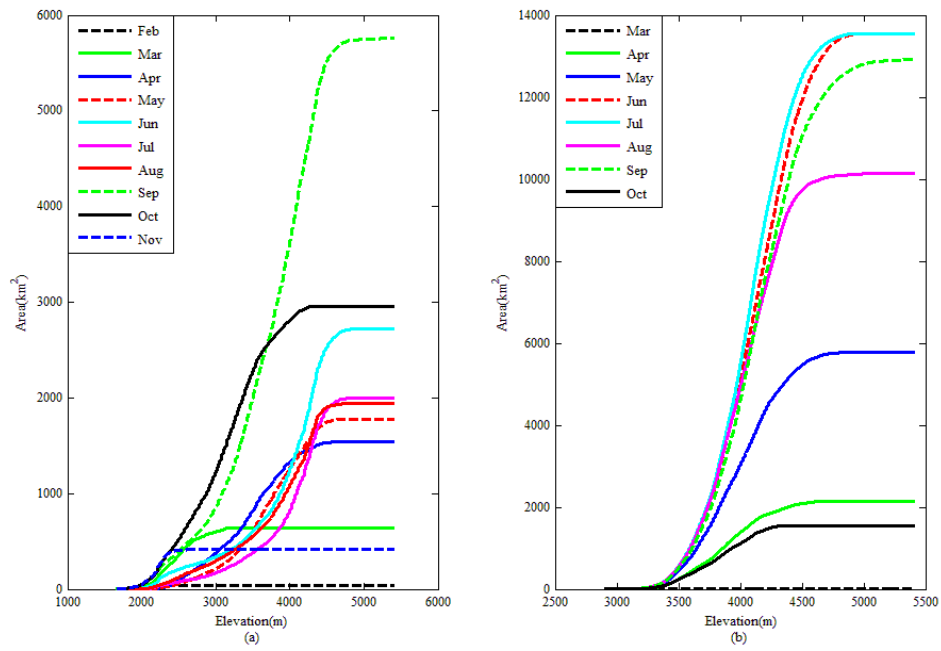
1083

1084 Figure 3. Proportion of monthly precipitation to annual amount (2003~2012). The red line in
 1085 each box represents the median value for each month from 2003 to 2012. Red crosses indicate
 1086 abnormal values that exceed 1.5 times the inter quartile range.



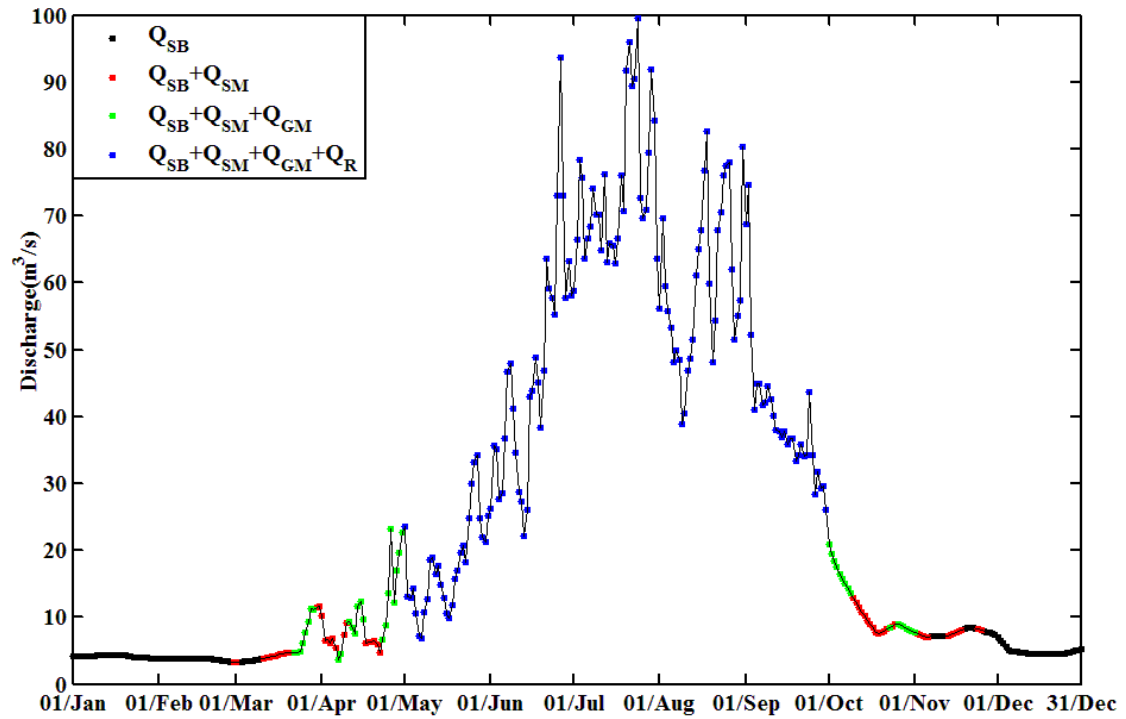
1087
 1088
 1089
 1090
 1091

Figure 4. Filtered MODIS eight-day snow-cover products (2004-2005). The term ‘mod’ is the snow cover area from MOD10A2 products, ‘myd’ is MYD10A2 products, ‘combined’ is the combined result from step1, ‘spatial-comb’ from step2 and ‘temporal-comb’ from step3. See Sect. 2.2.3 for details.



1092
 1093
 1094
 1095
 1096
 1097

Figure 5. Altitudinal Cumulative Melt Curve. (a) Cumulative monthly snowmelt area distribution by elevation (2003~2012). (b) Cumulative monthly glacier melt area distribution by elevation (2003~2012). The snowmelt areas in December and January and the glacier melt areas in November, December, January and February are zero and are not shown in this figure.



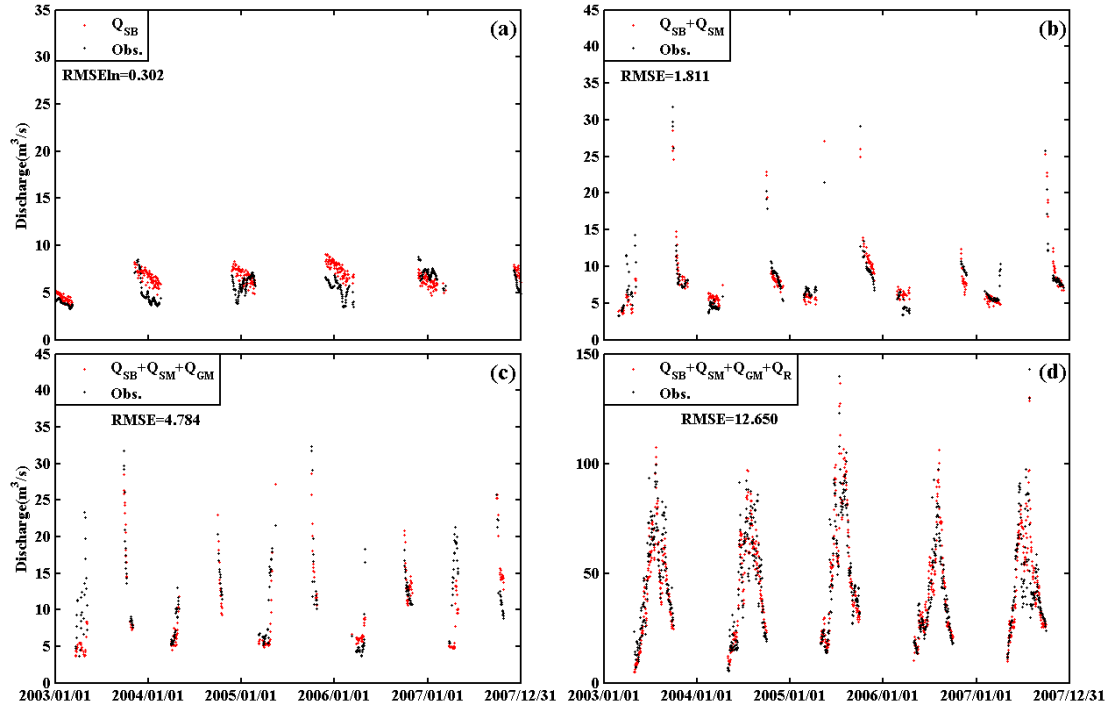
1098

1099

1100

1101

Figure 6. Hydrograph partition in 2003. Q_{SB} stands for subsurface baseflow generated by groundwater, Q_{SM} and Q_{GM} for snow meltwater and glacier meltwater respectively, and Q_R for rainwater directly runoff.



1102

1103

1104

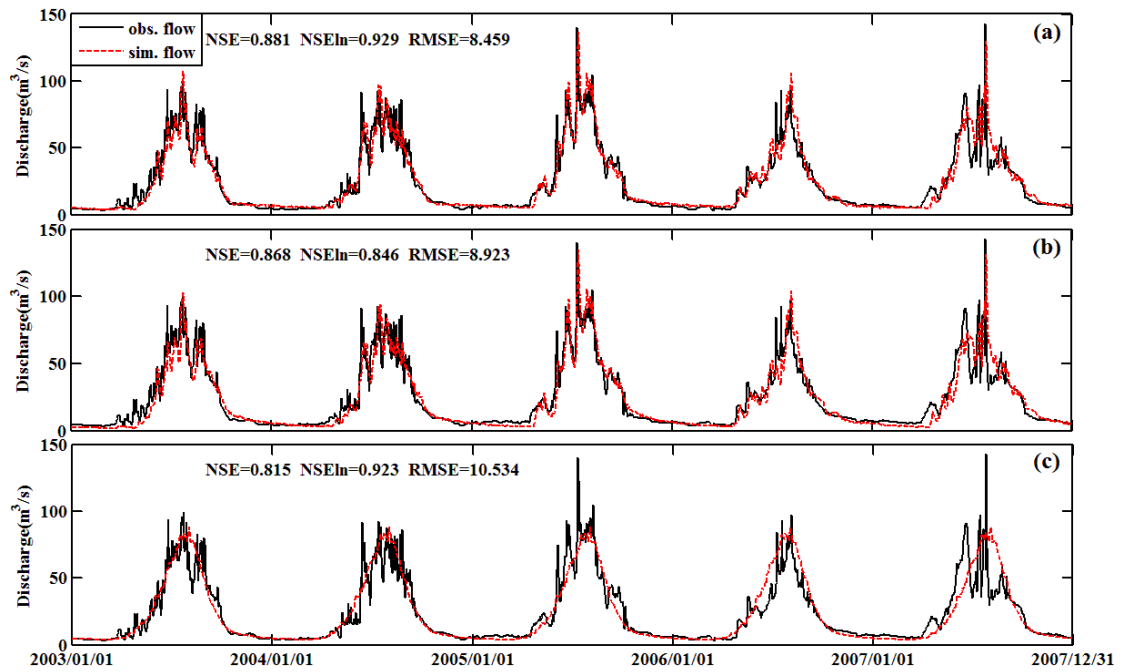
1105

1106

1107

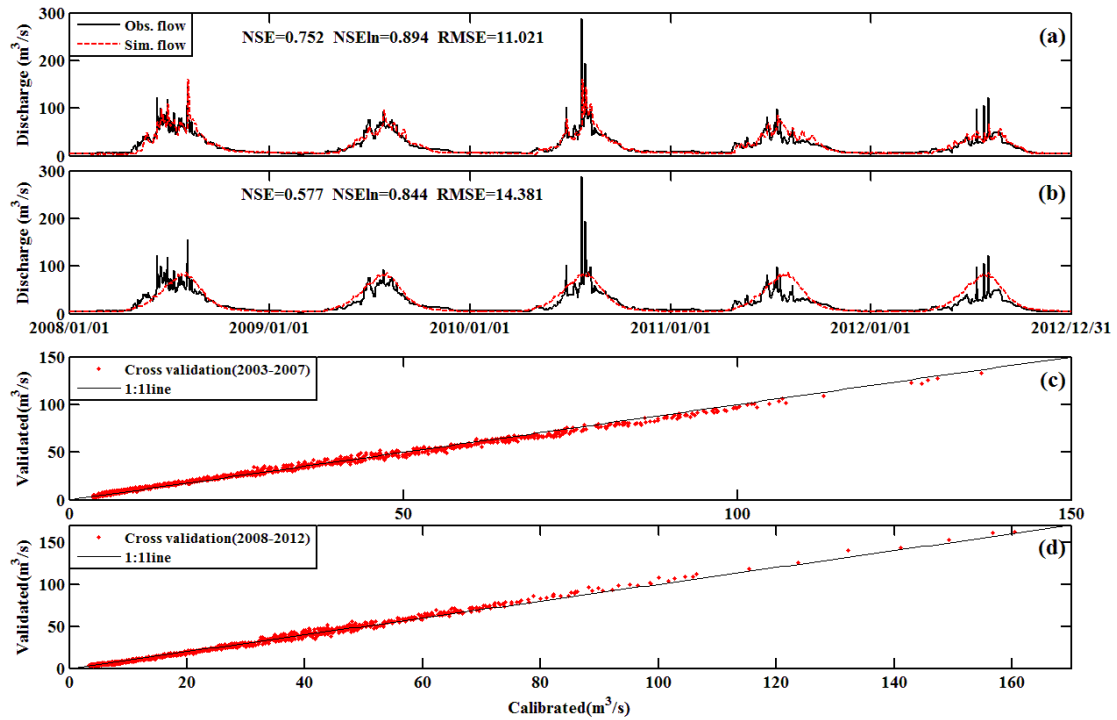
1108

Figure 7. Stepwise calibration of grouped parameters upon partitioning curves. (a) Partitioning curves after calibrating K_A and K_D upon Q_{SB} . (b) Partitioning curves after calibrating D_s upon $Q_{SB}+Q_{SM}$. (c) Partitioning curves after calibrating D_g upon $Q_{SB}+Q_{SM}+Q_{GM}$. (d) Partitioning curves after calibrating W_M and B upon $Q_{SB}+Q_{SM}+Q_{GM}+Q_R$. The goodness of fit between observed and simulated discharge is measured by $RMSEln$ (for Q_{SB} part) or $RMSE$ (for other parts).



1109
 1110
 1111
 1112

Figure 8. Simulation of daily streamflow by different methods from 2003 to 2007. (a) by the proposed stepwise method, (b) by the automatic calibration method, and (c) by the benchmark model. The performance of the simulations is measured in *NSE*, *NSEln* and *RMSE*.



1113

1114

1115

1116

1117

1118

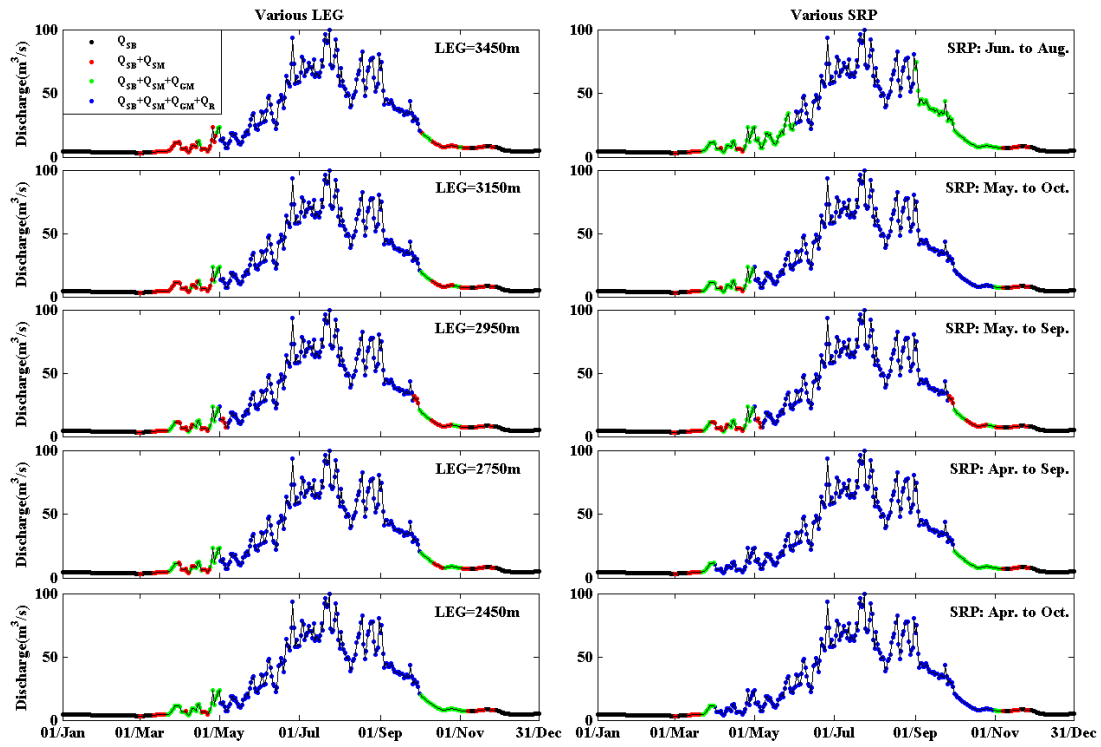
1119

1120

1121

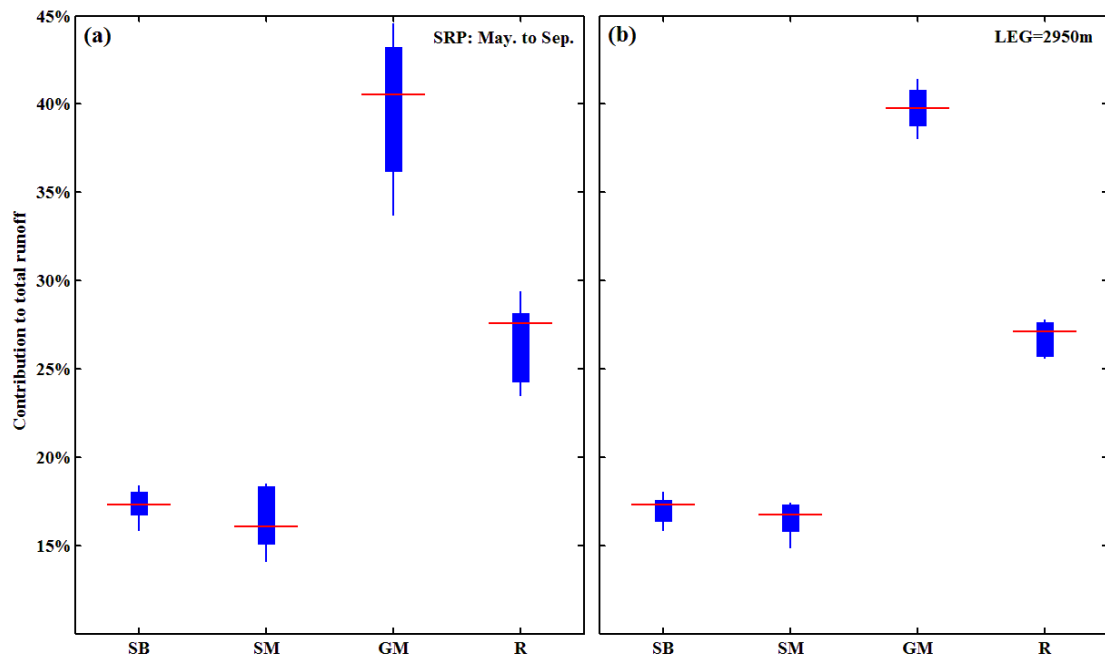
1122

Figure 9. Evaluation of the stepwise calibration method. (a) discharge simulation in evaluation period 2008 to 2012 using the stepwise calibrated parameters in calibration period 2003 to 2007. (b) discharge simulation in evaluation period 2008 to 2012 by the benchmark model. (c) Cross validation simulation of daily discharge in 2003-2007. x-coordinate presents the simulated daily discharges by parameters calibrated in period 2003-2007. y-coordinate presents the simulated daily discharges by parameters calibrated in period 2008-2012. (d) Cross validation simulation of daily discharge in 2008-2012. x-coordinate presents the simulated daily discharges by parameters calibrated in period 2008-2012. y-coordinate presents the simulated daily discharges by parameters calibrated in period 2003-2007.



1123
 1124
 1125
 1126
 1127

Figure 10. Sensitivity analysis for hydrograph partition. The first column is the hydrograph partition pattern using different lowest elevation band of the glacier area (LEG). The second column is the hydrograph partition pattern using different storm rain period (SRP).



1128

1129

1130

1131

1132

1133

1134

1135

Figure 11. Sensitivity analysis on the contributions of different runoff sources to total runoff. (a) is the contribution pattern under different lowest elevation band of glacier area (LEG), where the storm rain period (SRP) is fixed as May to September. (b) is the contribution pattern under different SRPs, where the LEG is fixed as 2950m. The red line stands for the mean contribution for each runoff source, and the top/bottom end of each plot presents the highest/lowest contribution ratio. SB is groundwater baseflow, SM is snowmelt, GM is glacier melt and R is rainwater directly runoff.